Polymer Chemistry

Suzuki-Miyaura Catalyst-Transfer Polymerization: New Mechanistic Insights

Journal:	*Polymer Chemistry*
Manuscript ID	PY-ART-05-2023-000580.R1
Article Type:	Paper
Date Submitted by the Author:	11-Aug-2023
Complete List of Authors:	Howell, Mitchell; Northern Illinois University, Chemistry & Biochemistry Kei, Peter; Louisiana State University, Chemistry Anokhin, Maksim; Northern Illinois University, Chemistry & Biochemistry Losovyj, Yaroslav; Indiana University Bloomington, Department of Chemistry; University of Nebraska-Lincoln, Department of Physics and Astronomy Fronczek, Frank; Louisiana State University, Chemistry Dept Nesterov, Evgueni; Northern Illinois University, Chemistry & Biochemistry; Louisiana State University, Chemistry

Suzuki-Miyaura Catalyst-Transfer Polymerization: New Mechanistic Insights

Mitchell T. Howell,[†] Peter Kei,[‡] Maksim V. Anokhin,[†] Yaroslav Losovyj,[§,#] Frank R. Fronczek,[‡] and Evgueni E. Nesterov[,†,‡]*

[†]Department of Chemistry and Biochemistry, Northern Illinois University, DeKalb, Illinois 60115, USA. E-mail: een@niu.edu

[‡]Department of Chemistry, Louisiana State University, Baton Rouge, Louisiana 70803, USA

[§]Department of Chemistry, Indiana University, Bloomington, Indiana 47401, USA

[#]Department of Physics and Astronomy, University of Nebraska, Lincoln, Nebraska 68588, USA

ABSTRACT. Controlled preparation of structurally precise complex conjugated polymer systems remains to be a major synthetic challenge still to be addressed, and this push is stimulated by the improved device performance as well as unique fundamental characteristics that the well-defined conjugated polymer materials possess. Catalyst-transfer polymerization (CTP) based on Pd-catalyzed Suzuki-Miyaura cross-coupling reaction is currently one of the most promising methods towards achieving such a goal, especially with the recent implementation of *N*-methyliminodiacetic acid (MIDA) boronates as monomers in CTP. Further expansion and development of practical applications of CTP methods will hinge on a clear mechanistic understanding of both the entire process and the particular

steps involved in the catalytic cycle. In this work, we introduced Ag^+-mediated Suzuki-Miyaura CTP and demonstrated that presence of Ag^+ shifted a key transmetalation step toward the oxo-Pd pathway, leading to direct participation of MIDA-boronates in the transmetalation step and hence in the polymerization process, and resulting in the overall more efficient polymerization. In addition, we found that, under Ag^+-mediated conditions, MIDA-boronates can also directly participate in small-molecule cross-coupling reactions. The direct participation of MIDA-boronates in Suzuki-Miyaura cross-coupling has not been envisaged previously and could enable new interesting possibilities to control this reaction both for small-molecule and macromolecular syntheses. In contrast to MIDA-boronates, boronic acid monomers likely undergo transmetalation through an alternative boronate pathway, although they may also be directed to react via the oxo-Pd transmetalation pathway in Ag^+-mediated conditions. The interplay between the two transmetalation pathways which are both involved in the catalyst-transfer polymerization, and the opportunity to selectively enhance one of them not only improves mechanistic understanding of Suzuki-Miyaura CTP process but also provides a previously unexplored possibility to gain more effective control over the polymerization to obtain structurally better-defined conjugated polymers.

Introduction

Controlled preparation of structurally precise and complex macromolecular systems represents one of the major synthetic challenges still to be addressed in the polymer field. In conjugated polymer (CP) research, the push to deliver macromolecular systems with structural accuracy reminiscent of a small-molecule synthesis is stimulated by the improved device performance as well as unique fundamental characteristics that the well-defined polymer materials may possess. Molecular weight, polydispersity, and precise incorporation of structural units in the conjugated backbone are among the important parameters that affect polymers' physical properties. For example, incorporation of a single electron-deficient perylenedicarboximide (PDCI) unit in a CP chain has been previously demonstrated to dramatically alter the polymer's optoelectronic properties, even when the CP materials were prepared using a non-precise, step-growth polymerization.[1-5] Although scientists cannot yet rival Nature in their ability to prepare structurally precise polymers, recent developments in various controlled or living chain-growth polymerization methods indicate that such a possibility is getting more realistic.[6-10] The field of conjugated polymers has recently experienced an impressive upswing toward the development of efficient controlled catalyst-transfer polymerization (CTP) protocols for the preparation of various classes of CPs.[11-15] Conjugated polymers are materials of choice for a breadth of potential practical applications in electronic, optoelectronic and sensing devices due to tunability of their optical and electronic properties through manipulations of the polymers' chemical structure. Whereas some classes of conjugated polymers (and block copolymers) can now be readily prepared using CTP methods, the real challenge remains in applying CTP for the preparation of more complex well-defined structures[16] (e.g. where a specific structural unit would be precisely incorporated in the CP chain – something that Nature routinely does with biopolymers). In addition, diversifying the range of monomers suitable for CTP beyond simple aromatic and heteroaromatic monocyclic structures is critical for the ability to prepare practically significant electronic and optoelectronic CP materials. Controlled polymerization has become a well-established method for preparing polythiophenes (PTs) and their block copolymers

following the milestone discovery by McCullough[17, 18] and Yokozawa[19, 20] that Ni^{II}-catalyzed Kumada coupling based polymerization of 5-bromo-2-thienylmagnesium monomers occurs as a quasi-living chain-growth process. The key features of this mechanism, including essential experimental evidence in favor of the principal role of the Ni^0 associated π-complex in maintaining the chain-growth process, have been studied in great detail,[21-25] and enabled expanding Kumada CTP to some other classes of conjugated polymers.[11]

These developments, however, resulted only in a limited expansion of the scope of CTP to more diverse and complex CPs required for modern materials applications, nor did it enable major expansion toward polymerization methods based on other transition metal catalyzed coupling reactions.[16, 26] The latter is particularly surprising considering steady advances made in designing highly efficient catalytic systems for a diverse multitude of cross-coupling reactions in the small-molecule synthesis field. Among such reactions, Pd-catalyzed Suzuki-Miyaura C–C cross-coupling stands out as an especially versatile process that occurs in mild reaction conditions and is highly functional group tolerant.[27-29] Not surprisingly, the polymer synthesis community has shown profound interest in exploring this reaction for the purpose of chain-growth catalyst-transfer polymerization.[30-39] Palladium is well suited to facilitate CTP process as it exhibits a lower aromatic ring-walking barrier,[40] and also lower binding affinity to N and O heteroatoms (which would allow expanding the range of suitable monomers for CTP).[41] Recent chemical literature describes many highly efficient Pd catalysts with various ligands that are suitable for cross-coupling of a diverse range of compounds. In the macromolecular field, however, the absolute majority of Suzuki-Miyaura CTP (SCTP) work employed Pd complexes with just a single ligand P(*t*-Bu)$_3$, utilized either as separately prepared external catalytic initiators Ar–Pd[P(*t*-Bu)$_3$]–X or the catalysts prepared *in situ* in the reaction of Ar–X with the Pd^0 complex, Pd[(*t*-Bu)$_3$]$_2$ (where Ar is an aryl group, and X is halogen).[31-38] Despite their popularity, P(*t*-Bu)$_3$-based Pd complexes are not ideal as they exhibit inconsistent initiation and CTP process suffers from frequent chain-transfer events, especially at the end of polymerization.[35, 42, 43] Another major problem with

conventional Suzuki-Miyaura CTP (SCTP) is that, in the coupling conditions requiring basic aqueous media, boronic acids and their derivatives used as monomers tend to undergo protodeboronation.[44, 45] Whereas this may present only a minor problem for small-molecule coupling, in SCTP it results in premature chain termination leading to lower yields and increasing dispersity index (*Đ*) of the CP product.[36, 37, 46] In 2015, Turner *et al.* reported on using *N*-methyliminodiacetic acid (MIDA) boronate ester **1** as a protected reactant capable of slow generation of the reactive boronic acid monomer in the SCTP conditions, thus allowing to circumvent the problem of protodeboronation.[47] They also attempted using one of the more efficient ligands, Buchwald's SPhos, along with $Pd_2(dba)_3$ to generate Pd precatalyst. These efforts yielded regioregular poly(3-hexylthiophene) (P3HT) polymer, however large dispersity (*Đ*) and modest molecular weight control indicated prevalence of the chain transfer and chain termination reactions.

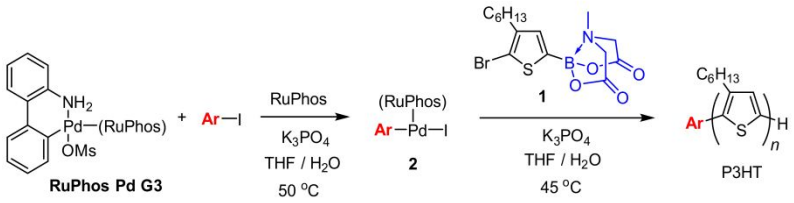

Fig. 1 Preparation of an external catalytic initiator **2** based on RuPhos Pd G3 precatalyst, and its use for SCTP of MIDA-boronate **1**.[48]

Taking on the same idea, in 2018 Choi *et al.* published a milestone report of SCTP utilizing thiophene MIDA-boronate **1** (Fig. 1).[48] They found that using an external catalytic initiator **2** prepared *in situ* by the reaction of the Buchwald's RuPhos Pd G3 precatalyst with substituted phenyl iodides produced P3HT with controllable molecular weight, consistently low dispersity and excellent yields (M_n up to 17.6 kDa, *Đ* >1.08, yield >90%). This report described the first robust and highly controlled chain-growth polymerization for the preparation of a conjugated polymer by SCTP. In the subsequent publications, the researchers have expanded this strategy towards some other simple boronate monomers

and demonstrated the great promise of both the Buchwald-type Pd catalytic systems and MIDA-boronate monomers for enhancing and facilitating SCTP process, including a controlled preparation of donor-acceptor CPs.[49-52] The continuing progress along this remarkably efficient polymerization protocol also underlined the need for better understanding of the still missing SCTP mechanistic details, especially when MIDA-boronate monomers are used, in order to apply a more rational approach toward optimization of reaction conditions and further improve the versatility and robustness of this promising macromolecular synthetic strategy. In this paper, we describe our studies of the SCTP polymerization mechanism with MIDA-boronate monomers, including the finding of their unexpected direct participation in the catalytic cycle, the role of the two transmetalation pathways in SCTP and the possibility to effectively control the polymerization through enforcing one of the two pathways.

Results and Discussion

Preparation of external catalytic initiator 3. Although previous SCTP works utilized *in situ* prepared external catalytic initiators which were used without isolation or purification (e.g. shown in Fig. 1), we decided to prepare, isolate, and structurally characterize the catalytic initiator prior to polymerization studies. We assumed that using pure and structurally homogeneous catalyst would facilitate subsequent SCTP and help in further mechanistic studies. The catalytic initiator **3** was prepared in 92% yield using the reaction of Buchwald's RuPhos Pd G3 palladacycle with 2-iodotoluene (Fig. 2a). The *o*-tolyl unit has been chosen due to its lower propensity towards disproportionation (homocoupling) in **3**. The crude **3** was purified via recrystallization from hexanes, which provided crystalline material suitable for X-rays crystallographic studies (Fig. 3). Both the crystal structure and ^{1}H NMR spectrum (Fig. S16 in the ESI) showed the incorporation of co-crystallized carbazole (which is a by-product of the formation of **3** from RuPhos Pd G3) in a 1:1 ratio with **3**. In good agreement with the previous studies of similar compounds,[53, 54] the central Pd atom showed a nearly square planar

geometry, and π-bonding with one of the phenyl rings in the RuPhos ligand (π-bond length 2.46 Å). The ability to encounter well-defined π-complexation with an aromatic ring is a major prerequisite for efficient Pd association with the π-conjugated chain in the catalyst-transfer step and is required for robustness of the chain-growth polymerization mechanism. A single RuPhos ligand therefore acts as a bidentate ligand and provides needed coordination to stabilize the Pd complex and all the intermediates participating in the SCTP catalytic cycle, without the need for any additional ligand.

Whereas preparing catalytic initiator **3** starting from RuPhos Pd G3 precursor is a straightforward and simple approach, the simultaneous formation of the by-product carbazole leads to its presence in subsequent polymerization reactions, even when a sample of **3** was recrystallized prior to polymerization. Previous studies have reported on possible retarding effect of carbazole when it was present during Suzuki-Miyaura cross-coupling,[55] therefore it was prudent also to prepare a carbazole-free catalytic initiator **3** for comparison experiments An efficient alternative route is outlined in Fig. 2b and based on the recently reported procedure by Buchwald *et al.*[56] Reaction of COD-palladacycle **4** with RuPhos and small excess of 2-iodotoluene furnished the required catalytic initiator **3** in 75% yield after recrystallization. The additional advantage of this procedure over the one shown in Fig. 2a is the possibility to prepare different catalytic initiators with a range of phosphine ligands starting from a single palladacycle compound **4**.

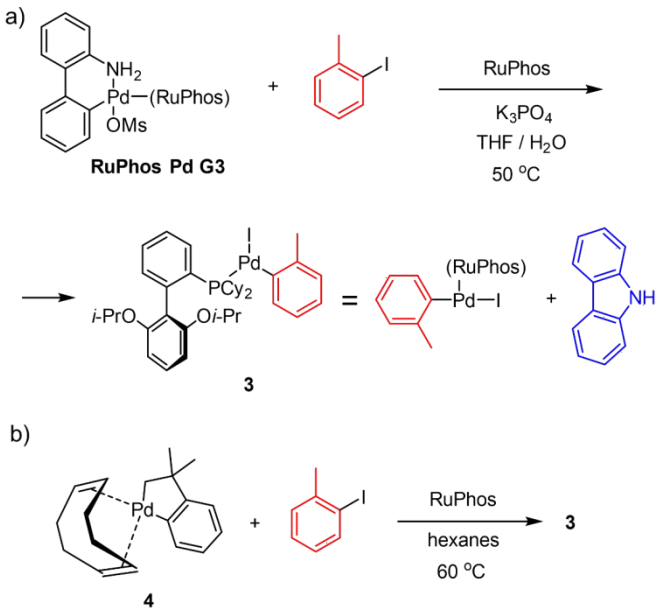

Fig. 2. a) Preparation of the external catalytic initiator **3** using RuPhos Pd G3 precursor. This route involves formation of by-product carbazole which co-crystallizes with target compound **3**. b) An alternative route to **3** resulting in no carbazole by-product.

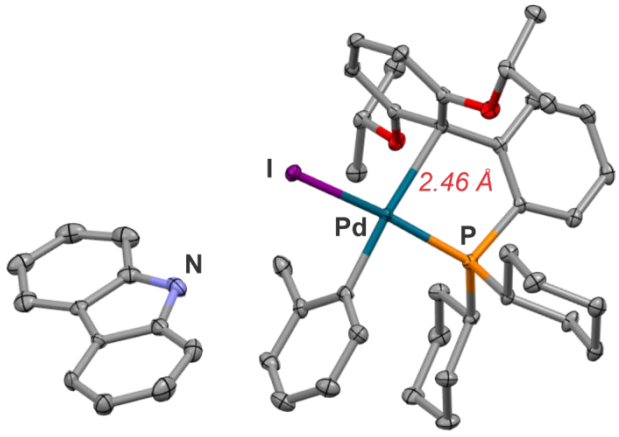

Fig. 3. Ellipsoid drawing at the 50% level, representing crystal structure of external catalytic initiator **3**. Hydrogen atoms are omitted for clarity; the carbazole molecule is disordered over two positions, with only one position shown.

Ag^+-mediated polymerization of MIDA-boronate monomer 5. As a monomer for polymerization studies, we chose fluorenyl MIDA-boronate monomer **5** (Fig. 4). The rationale for selecting the fluorenyl monomer was two-fold. First, we would like to use a monomer without a

heteroatom in the aromatic ring, as heteroaromatic compounds, such as thiophene, typically show better ability to bind with Pd^0 centers which leads to improved Pd^0 ring-walking and higher catalyst-transfer polymerization efficiency overall, whereas mechanistic studies would benefit from a more "mediocre" monomer as variation of reaction conditions should result in noticeably dramatic changes between the polymerization outcomes. Second, the two phenylene rings per each monomer unit would necessarily slow down the catalyst-transfer process, again making the polymerization process of this monomer less controlled than, for example, thiophene monomers. In a recent study,[57] Yokozawa has demonstrated that in the SCTP process, Pd^0 catalyst transfer step over thiophene repeating units was substantially more efficient as compared to the catalyst transfer over fluorene units. Thus, the intrinsically lower chain-growth polymerization efficiency with the fluorenyl monomer would make the process more sensitive to the effect of reaction conditions and should reveal more subtle mechanistic details of the polymerization process.

Table 1. Initial studies on externally initiated SCTP of MIDA-boronate monomer **5**. [a]

Entry	M_0/I_0 [b]	Base (eq.)	Ag^+ source	Ag^+ (eq.)	Time, (h)	Yield (%)	M_n [c] (kDa)	M_w [c] (kDa)	$Đ$ [c]
1	16:1	K_3PO_4 (10)	–	0	48	12	3.2	3.9	1.24
2	16:1	K_3PO_4 (10)	Ag_2SO_4	1	48	60	5.6	7.1	1.28
3	16:1	K_3PO_4 (10)	AgOAc	1	48	50	6.5	9.1	1.27
4	16:1	K_3PO_4 (10)	$AgNO_3$	1	48	57	6.4	9.0	1.40
5	16:1	K_3PO_4 (10)	Ag_2CO_3	1	48	50	6.0	8.0	1.34
6	16:1	K_3PO_4 (10)	$AgBF_4$	1	48	43	6.0	8.0	1.33
7	16:1	K_3PO_4 (10)	AgOTf	1	48	47	6.6	9.5	1.44
8	16:1	K_3PO_4 (10)	Ag_2O	1	48	16	3.6	4.0	1.12
9	16:1	K_3PO_4 (10)	AgBr	1	48	16	4.0	4.7	1.16
10	48:1	K_3PO_4 (10)	Ag_2SO_4	1	48	31	10.8	15.8	1.46

11	48:1	KOAc (10)	Ag_2SO_4	1	48	<1	–	–	–
12	48:1	K_3PO_4 (10) [d]	Ag_2SO_4	1	48	22	7.0	9.0	1.29
13	48:1	CsOH (10)	Ag_2SO_4	1	48	13	9.4	25.9	2.75
14	48:1	Cs_2CO_3 (10)	Ag_2SO_4	1	48	34	11.7	15.4	1.32
15	48:1	Cs_2CO_3 (1)	Ag_2SO_4	1	48	<1	–	–	–
16	48:1	Cs_2CO_3 (5)	Ag_2SO_4	1	48	16	5.8	6.5	1.13
17	48:1	Cs_2CO_3 (15)	Ag_2SO_4	1	48	22	8.1	10.3	1.26
18	48:1	Cs_2CO_3 (20)	Ag_2SO_4	1	48	12	6.2	7.6	1.23
19 [e]	48:1	Cs_2CO_3 (10)	Ag_2SO_4	1	48	39	7.8	14.6	1.87
20 [e]	48:1	Cs_2CO_3 (10)	Ag_2SO_4	1	24	34	10.0	17.4	1.74
21 [f]	24:1	Cs_2CO_3 (10)	Ag_2SO_4	1	42	46	8.3	14.8	1.78
22 [f]	24:1	Cs_2CO_3 (10)	–	0	42	18	3.5	3.9	1.11

[a] Reaction conditions: temperature 30 °C (except entries 19 and 20), solvent THF with 5% v/v water, catalytic initiator **3** containing 1 eq. of carbazole, the amounts of Ag^+ and Cs_2CO_3 are provided with respect to monomer **5**; [b] Monomer **5** to catalytic initiator **3** ratio; [c] Determined with GPC using THF as eluent and calibrated against polystyrene standards; [d] With added 18-crown-6; [e] Polymerization was performed at 40 °C; [f] Polymerization was carried out in the presence of 0.5 eq. of added RuPhos phosphine ligand.

Throughout most of these studies, we used catalytic initiator **3** containing 1 eq. of carbazole (i.e. prepared as indicated in Fig. 2a) as was customarily used in all previously reported works. We first attempted polymerization of monomer **5** using conditions similar to those developed by Choi *et al.* for thiophene monomer **1** (i.e. using 10 eq. K_3PO_4 as base and 5% v/v solution of H_2O in THF as solvent), with monomer **5** to catalytic initiator **3** (M_0/I_0) ratio of 16:1. This run is shown as entry 1 in Table 1. It was expected that slow hydrolysis of MIDA-boronate group would result in a near steady-state concentration of the corresponding boronic acid that would undergo SCTP process. Although the experiments with 48 h polymerization time resulted in a polyfluorene (PF) polymer with relatively narrow dispersity ($Đ$ 1.24) indicating controlled chain-growth mechanism, the molecular weight was below theoretically predicted for this M_0/I_0 ratio (M_n 3.2 kDa vs. theoretical M_n 6.2 kDa), and the yield

was also low (12%). Thus, the experimental conditions optimized for the preparation of polythiophenes were not well suited for the polymerization of fluorene monomer **5** and reflected poor efficiency of at least one step in the catalytic cycle involving this monomer.

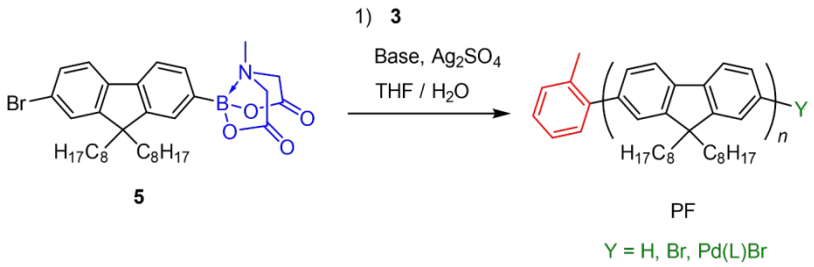

Fig. 4. Externally-initiated polymerization of MIDA-boronate monomer **5**. Ag_2SO_4 was not used in all runs (see Table 1 for specific experimental details). Ligand L is RuPhos.

Although catalytic cycle for Pd-catalyzed Suzuki-Miyaura (SM) cross-coupling involving boronic acids and aryl halides has been extensively studied, the nature of the transmetalation step remains controversial. Originally, two alternative routes have been debated for this step: the boronate pathway, and the oxo-Pd pathway (Fig. 5).[58] Because SM coupling occurs in basic conditions, it has been postulated that formation of the tetracoordinate boronate "ate" complex $[Ar–B(OH)_3]^-$ from the reaction of boronic acid with hydroxide anion precedes transmetalation, and this is followed by the boronate nucleophilic attack at the arylpalladium halide complex. Alternatively, in the oxo-Pd pathway, conversion of the arylpalladium halide to ArPd–OH complex happens first, followed by the nucleophilic attack at the neutral boronic acid. Although both pathways would result in the same Pd–O–B pre-transmetalation intermediate, the efficiency of each of them could be dramatically different. Indeed, in 2011 Amatore[59] and Hartwig[60] independently demonstrated that the oxo-Pd pathway was kinetically faster than the boronate pathway, and since then it was almost universally accepted that the transmetalation step in SM cross-coupling occurs via the oxo-Pd pathway. Nevertheless, there is a significant amount of research pointing to occurrence of transmetalation through the boronate

pathway,[61, 62] including a recent study by Denmark *et al.*[63] The mechanistic investigations on the transmetalation step are often complicated by the biphasic, heterogeneous reaction conditions in SM cross-coupling and that many of the studies have been done in stoichiometric rather than catalytic conditions. Thus, it appears that, depending on reaction conditions, SM cross-coupling can involve either boronate or oxo-Pd transmetalation step.

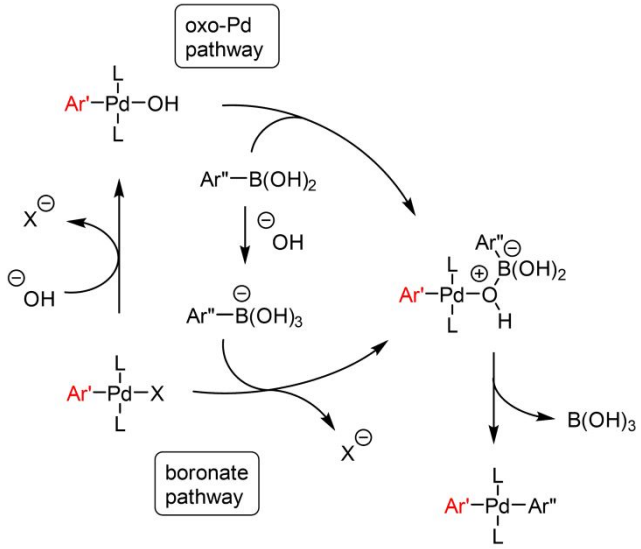

Fig. 5. Two alternative pathways (boronate and oxo-Pd) leading to the transmetalation step in SM coupling mechanism.

If we assume that SM cross-coupling occurs through a more efficient oxo-Pd transmetalation pathway, and there is an equilibrium between ArPd–X (boronate pathway intermediate) and ArPd–OH (oxo-Pd pathway intermediate) complexes, then it would be possible to shift the equilibrium toward ArPd–OH complex and hence enforce the oxo-Pd pathway through effective removal of the halide anion.[64] This could be done via addition of Ag^+ cations that would react with halide to form insoluble AgX. As a source of Ag^+, we first chose Ag_2SO_4 due to its moderate solubility in the aqueous THF reaction medium, which would enable slow delivery of Ag^+ during the reaction and preclude rapid formation of an insoluble Ag_2O precipitate.

Adding 1 eq. of Ag^+ (i.e. 0.5 eq. of Ag_2SO_4) resulted in dramatic improvement of the monomer **5** polymerization outcome (entry 2 in Table 1): the PF molecular weight M_n increased to near-theoretical 5.6 kDa with low dispersity ($Đ$ 1.28), and overall 60% yield. This was the first demonstration that adding equimolar Ag^+ could improve the SCTP process possibly through enforcing the oxo-Pd transmetalation pathway.

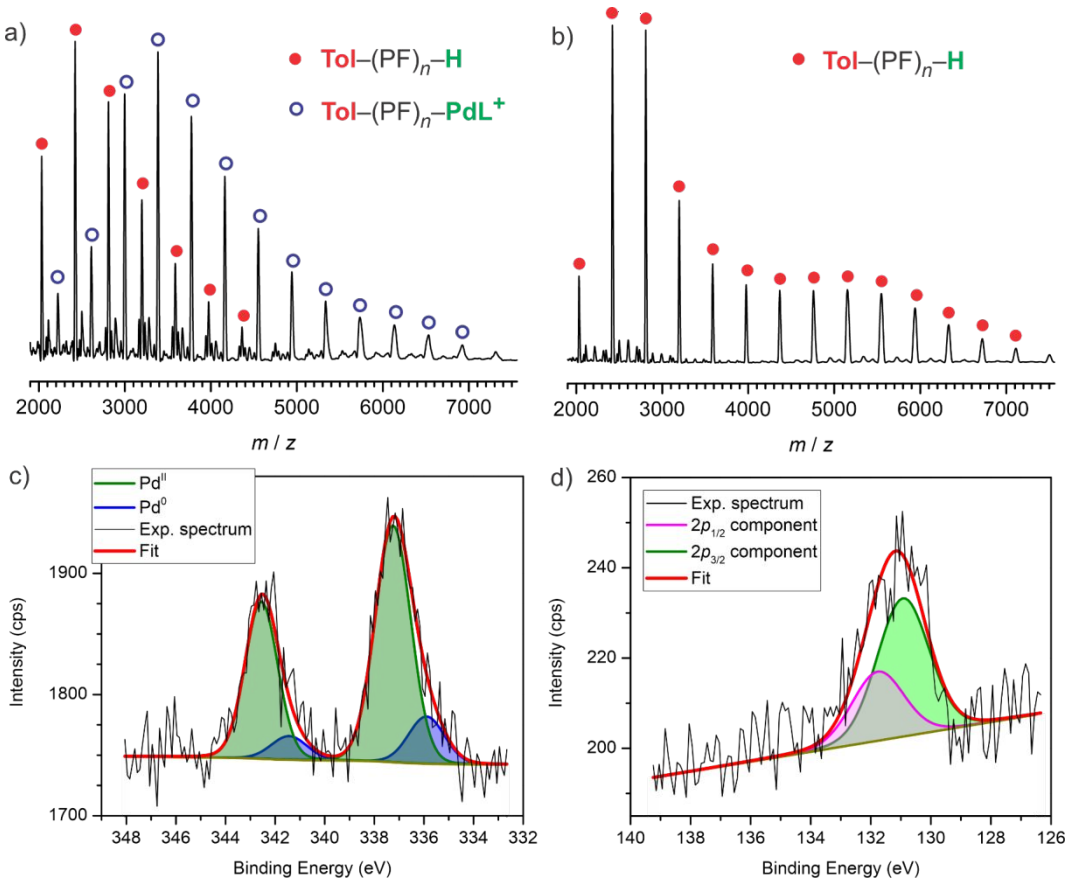

Fig. 6. a) MALDI-TOF data for PF polymer in entry 2 of Table 1. Milder workup conditions (6 N HCl, room temperature, 1 h) were used for this sample; L is RuPhos ligand. b) MALDI-TOF data for the polymer in (a) after a more vigorous workup (12 N HCl, 45 °C, 1 h). c) and d) High-resolution Pd 3*d* (c) and P 2*p* (d) XPS spectra of a drop-cast film of polymer in (a). Deconvolution into Pd^{II} and Pd^0 components is shown for Pd spectrum, and deconvolution to $2p_{1/2}$ and $2p_{3/2}$ components is shown for P spectrum. Shirley background (yellow traces) was applied to the spectra.

An interesting observation was made upon analysis of MALDI-TOF data for the PF polymer in entry 2. The mass spectral analysis is used to evaluate end-group composition of the polymers and can

provide useful information about the polymerization mechanism. Assuming the controlled chain-growth mechanism, the polymer chains should be terminated with an *o*-tolyl group (from catalytic initiator **3**) on one chain end, and with H or Br on the other chain end (resulting from the acid-promoted removal of the active Pd center upon acidic post-polymerization workup). Such polymers would be referred to as Tol–$(PF)_n$–H or Tol–$(PF)_n$–Br, respectively. Initially, we used a relatively mild post-polymerization workup involving adding 6 N HCl to the reaction and stirring the resulting mixture at room temperature for 1 h. To our surprise, MALDI-TOF analysis showed predominant composition of detected polymer chains as Tol–$(PF)_n$–PdL^+, where L is a RuPhos ligand (Fig. 6a). Since loss of a halide anion could happen during MALDI ionization, the likely initial composition of such chains can be described as Tol–$(PF)_n$–Pd(L)Br. More vigorous acidic workup conditions (adding 12 N HCl with subsequent stirring at 45 °C for 1 h) resulted in disappearance of the Pd(L)Br end groups, yielding the predominant polymer composition Tol–$(PF)_n$–H (Fig. 6b). To further confirm the presence of the Pd(L)Br end groups and investigate electronic nature of the Pd atom, we carried out X-ray Photoelectron Spectroscopy (XPS) study on drop-cast films of the polymer obtained upon mild workup conditions. The XPS signal of Pd (3*d* line) showed a dominating component corresponding to Pd^{II} (characteristic signals at 337 and 343 eV, Fig. 6c), thus confirming it as a product of oxidative addition of Pd at the terminal C–Br bond. XPS study also confirmed that Pd had an associated phosphine ligand, as a clear P 2*p* signal was observed at 131 eV (Fig. 6d). This confirmed that the polymer chains isolated after the polymerization reaction and mild acidic workup had the composition Tol–$(PF)_n$–Pd(L)Br (where L is RuPhos ligand). Successful isolation during CTP of the "living" polymer chains terminated with active metal centers has been recently demonstrated in other systems. For example, Seferos *et al.* have isolated Ni^{II}-terminated polymer chains in the case of Kumada CTP of thiophene monomers,[65] and Buchwald *et al.* have observed Pd^{II}-terminated chains in the case of SCTP of pyridine monomers.[66] From a mechanistic standpoint, the isolation of the relatively stable Tol–$(PF)_n$–Pd(L)Br complex upon completion of polymerization (rather than Tol–$(PF)_n$–Pd(L)–OH) indicated that it was likely the resting

state of polymerization, with the rate-determining step being conversion of the less reactive Tol–$(PF)_n$–Pd(L)Br to the more reactive Tol–$(PF)_n$–Pd(L)–OH intermediate. Therefore, improvement of the polymerization outcome through addition of Ag^+ was due to enforcing the oxo-Pd pathway.

We also investigated the effect of the nature of Ag^+ source on polymerization of **5**. In addition to Ag_2SO_4, we attempted using silver acetate, silver nitrate, silver carbonate, silver tetrafluoroborate, and silver triflate (entries 3-7 in Table 1). The results with all salts were comparable with respect to the polymer yield and molecular weight. For some more soluble salts ($AgNO_3$ and AgOTf) we observed some modest increase in dispersity. In contrast, completely insoluble Ag^+ sources, Ag_2O and AgBr, resulted in essentially no change relative to a Ag^+-free case in entry 1 (entries 8 and 9 in Table 1). By comparison of all results, Ag_2SO_4 demonstrated overall better performance, and it was retained for the rest of this study.

Increasing the ratio of monomer **5** to catalytic initiator **3** (M_0/I_0) to 48:1 resulted in PF polymer with an expectedly higher molecular weight, albeit with somewhat higher dispersity (M_n 10.8 kDa, $Đ$ 1.46, entry 10 in Table 1). Noticeably, the polymer yield dropped to about 30% indicating that not all monomer **5** was able to react; the lower polymer yields will be addressed in more detail later in the paper. Since base plays an important role in SM cross-coupling, we studied the effect of replacing K_3PO_4 with alternative bases. Potassium acetate did not result in formation of polymer (entry 11 in Table 1), whereas using K_3PO_4 together with 18-crown-6 resulted in a polymer with lower molecular weight (entry 12 in Table 1). Introducing a very strong base (CsOH) had an adverse effect on polymerization, producing a lower yield of polymer with high dispersity ($Đ$ 2.75, entry 13 in Table 1). On the other hand, using a moderately stronger base Cs_2CO_3 resulted in some improvement of the polymerization outcome compared to the case of K_3PO_4 base (entry 14 in Table 1 and Fig. S1 in the ESI). Therefore, we decided to switch to Cs_2CO_3 base for the subsequent experiments.

The base performs multiple functions in SM cross-coupling and hence in SCTP process. Therefore, we elucidated the effect of the amount of base (varied from 1 to 20 eq.) on the Ag^+-mediated

SCTP (entries 14-18 in Table 1). Both yield and molecular weight passed through a maximum at 10 eq. of Cs_2CO_3 while still maintaining a reasonably low dispersity. The increase in base concentration (corresponding to increasing HO^- activity in THF phase) improving the SCTP outcome could be linked to promoting formation of the active oxo-Pd complex ArPd(L)–OH, whereas adverse effect at even higher base concentrations could be related to the formation of the less reactive boronate intermediate $[ArB(OH)_3]^-$. Notice that this explanation is solely based on the common assumption that MIDA-boronate monomer **5** must first hydrolyze to the corresponding free boronic acid monomer which then undergoes transmetalation in the oxo-Pd pathway. Our subsequent kinetic studies, however, made this assumption questionable (*vide infra*).

In the optimization study, we checked the effect of higher reaction temperature (40 °C) on the SCTP outcome (entries 19-20 in Table 1). As anticipated, increasing reaction temperature resulted in the polymers with substantially broader dispersity ($Đ$ >1.70) without noticeable polymer yield improvement, indicating potential dissociation of the Pd^0 π-complex during polymerization, with subsequent Pd transfer to monomer and initiation of the new polymer chains (and hence loss of controlled nature of the polymerization process). While other factors beyond chain transfer might also result in broader dispersity, MALDI-TOF mass spectral analysis of the polymer in entry 19 indicated substantial presence of the chains with $(HO)_2B–(PF)_n–H$ composition likely resulting from Pd^0 transfer to the monomer **5** (Fig. S2 in the ESI).

Finally, we examined the impact of excess RuPhos ligand on the polymerization as previous reports had indicated that using excess phosphine ligand would improve control over SCTP.[30, 67] The polymerization runs of monomer **5** were carried out at M_0/I_0 ratio of 24:1 (entries 21 and 22 in Table 1). When the polymerization using catalytic initiator **3** was done without Ag_2SO_4 but with 0.5 eq. of added RuPhos ligand (entry 22), the low molecular weight polymer was obtained similar to the run in entry 1, indicating inefficient chain-growth polymerization. MALDI-TOF analysis of this sample revealed a large fraction of the polymer chains with composition $H–(PF)_n–H$ and $H–(PF)_n–Br$, resulting from

prevalent chain-transfer events (Fig. S3 in the ESI). When polymerization with 0.5 eq. excess RuPhos ligand was carried out in the presence of Ag_2SO_4 (entry 19), a polymer with M_n 8.3 kDa and broad dispersity ($Đ$ 1.78) was obtained. Similar to the case of polymerization at a higher temperature, this possibly resulted from an enhanced chain-transfer process rendering less controlled character of the polymerization. This was confirmed via MALDI-TOF mass spectral analysis of the polymer sample that revealed presence of the chains with H–$(PF)_n$–H composition (Fig. S4 in the ESI). Based on our observations, we hypothesized that excess ligand in this case could interact with Ag^+ leading to formation of an active complex that might interfere with chain-growth polymerization mechanism. Indeed, ^{31}P NMR monitoring of the reaction upon addition of 1 eq. of Ag_2SO_4 to RuPhos in the presence of Cs_2CO_3 indicated a downfield shift of the ^{31}P signal (from –8.9 to 21.1 ppm) which also became a doublet with a large coupling constant of 764 Hz, due to ^{31}P – ^{107}Ag coupling (Fig. S5 in the SI).[68] Although we did not further investigate the role of the Ag^I-RuPhos complex formation, its interference with the polymerization could explain why we did not observe any beneficial effect of adding excess RuPhos.

Pd^{II} species formed in the reaction with Ag^+ and their interconversion. In order to better understand the role of added Ag^+ in facilitating SCTP of MIDA-boronate monomer **5**, we decided to study in more detail what happened when Ag_2SO_4 was added to catalytic initiator **3**. Initially, we used initiator **3** prepared according to the route shown in Fig. 2a (i.e. containing co-crystallized carbazole). First, using ^{31}P NMR spectroscopy, we observed that adding a 10 eq. excess of Ag_2SO_4 to a solution of catalytic initiator **3** in aqueous THF solvent in the presence of Cs_2CO_3 base resulted in a noticeable shift of the singlet at 24.8 ppm (corresponding to **3**) to 29.3 ppm (Fig. S5 in the ESI). Subsequently, we were able to isolate and purify the new product via recrystallization, and the analysis of its ^1H NMR spectrum indicated the presence of carbazole signals. Crystals suitable for X-ray crystallographic study were obtained by slow evaporation from a hexanes-THF solution, and revealed that the new product was Pd-carbazolide **6** (Fig. 7a, b). Similar Pd^{II}-amido complexes have been considered key intermediates in

Buchwald-Hartwig Pd-catalyzed amination reactions.[69-71] Such compounds are usually quite stable at room temperature and only slowly undergo reductive elimination at relatively high temperatures.[69] However, their formation typically requires adding a strong base (e.g. sodium *tert*-butoxide) to initially deprotonate the amine. It is less likely that a weaker base Cs_2CO_3 could effectively deprotonate carbazole (pK_a 19.9[72]) and therefore the observed facile formation of **6** required certain participation of Ag^+. We hypothesized that the Pd-carbazolide complex was formed as a result of interaction of carbazole with a cationic Pd^{II} intermediate obtained upon removal of iodide from **3** (Fig. 7a) followed by deprotonation of the relatively acidic carbazolium species to form **6**. The Pd^{II}-amido complexes like **6** have been considered relatively unreactive and hence responsible for retardation of SM cross-coupling when it was carried out in the presence of compounds bearing azole heterocycles with relatively high N–H acidity (i.e. with pK_a values below that of pK_a of water).[73] Facile formation of the complex **6** in the Ag^+-mediated conditions illustrated that the carbazole by-product obtained in the typical process of generation of the catalytic initiator **3** from the RuPhos Pd G3 precursor would not necessarily be an "innocent" bystander but could influence the course of the cross-coupling reaction. Specifically, it brought about the question of what species was indeed acting as a catalytic initiator in the Ag^+-mediated SCTP reactions described above, especially considering the presumed low reactivity of **6**.

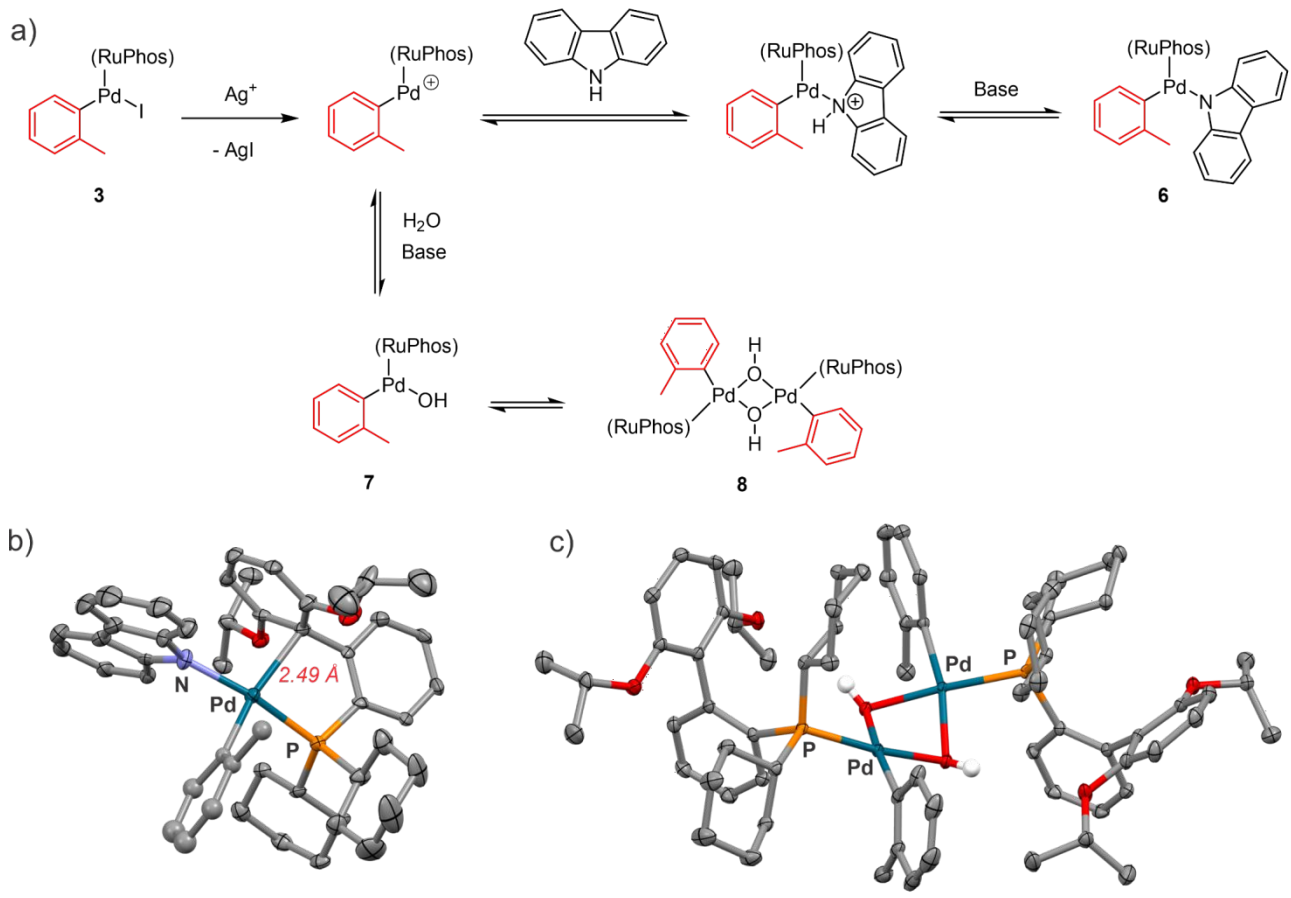

Fig. 7. a) Interconversion of various compounds generated from catalytic initiator **3** in Ag^+-mediated reaction conditions. b) Ellipsoid drawing at the 50% level, representing crystal structure of Pd-carbazolide **6**. Hydrogen atoms are omitted for clarity; the *o*-tolyl group was disordered over two conformations, with only the major conformer shown. c) Ellipsoid drawing at the 50% level, representing crystal structure of hydroxo-Pd dimer **8**. Hydrogen atoms are omitted for clarity except for the two OH hydrogens.

At that point, we decided to study reactivity of the carbazole-free catalytic initiator **3** (prepared as outlined in Fig. 2b) in Ag^+-mediated conditions. We observed exclusive formation of hydroxo-Pd complex **7** when the carbazole-free precursor **3** was reacted with 1 eq. Ag_2SO_4 in aqueous (5% v/v water) THF in the presence of Cs_2CO_3. The completeness of this conversion was monitored by ^{31}P NMR spectra where the disappearance of the initial peak at 24.8 ppm was accompanied by appearance of a new peak at 36.7 ppm (Fig. S5 in the ESI). The obtained product displayed a characteristic Pd–OH signal at –2.1 ppm in ^1H NMR spectrum (Fig. S21 in the ESI).[74] Slow recrystallization of **7** from

hexanes-THF solution produced crystals suitable for an X-ray crystallographic study which revealed the formation of ArPd(L)–OH dimer **8** (Fig. 7c). Due to the ability of RuPhos ligand to act both as a monodentate and bidentate ligand, the complex **7** and its dimer **8** can exist in equilibrium. Formation of dimer **8** was likely upon crystallization, whereas ^{1}H NMR spectrum of the solution was more consistent with the monomeric ArPd(L)–OH complex **7**.

With the complexity of different Pd^{II} species present in the Ag^{+}-mediated SCTP conditions, we evaluated the ability of each of the obtained complexes to act as catalytic initiators for SCTP of MIDA-boronate monomer **5** (Table 2). In comparison to the reference catalytic initiator **3** containing co-crystallized carbazole (entry 1), the Pd complex **3** (carbazole-free) and presumably "unreactive" Pd-carbazolide complex **6** (entry 3 in Table 2) all produced PF polymers with similar characteristics. The invariability of the polymerization results indicated that in the Ag^{+}-mediated reaction conditions, regardless of the initially taken catalytic initiator, all the Pd complexes equilibrated to produce the same actual catalytic initiator of the SCTP process. The remarkable outlier was the hydroxo-Pd complex **7** that produced PF polymer with narrow dispersity and the higher molecular weight closer to the theoretical value (entry 4 in Table 2, theoretical M_n 9.3 kDa). The obvious improvement of the polymerization outcome with complex **7** could indicate that it was this compound that was acting as the actual catalytic initiator in the Ag^{+}-mediated polymerization conditions and that using this compound as an SCTP catalytic initiator should benefit the polymerization. This hypothesis was in line with our original conjecture that adding Ag^{+} to the reaction medium would shift the transmetalation step toward the more efficient oxo-Pd pathway. Therefore we concluded that, independent on the Pd complex taken as a catalytic initiator (and on the presence or absence of carbazole), the actual catalytic initiator in the Ag^{+}-mediated SCTP was the ArPd(L)–OH complex formed *in situ* in the reaction conditions. Whereas hydroxo-Pd complex **7** seemed to provide a better polymerization outcome when used as a catalytic initiator, for uniformity of the results and to simplify the discussion, we decided to stay with the catalytic initiator **3** co-crystallized with carbazole for the subsequent studies described in this work (unless where

using a carbazole-free initiator is specifically mentioned), and to investigate using hydroxo-Pd complex as a catalytic initiator for Ag^+-mediated SCTP as part of a separate study to be published in due course.

Table 2. Ag^+-mediated SCTP of MIDA-boronate monomer **5** in the presence of different Pd catalytic initiators. [a]

Entry	Catalyst	Yield (%)	M_n [b] (kDa)	M_w [b] (kDa)	$Đ$ [b]
1	**3** (with carbazole)	34	6.1	7.6	1.24
2	**3** (carbazole-free)	39	6.3	8.8	1.41
3	**6**	39	5.9	7.5	1.28
4	**7**	40	8.2	10.4	1.27

[a] Reaction conditions: temperature 30 °C, reaction time 42 h, monomer to initiator **5** ratio (M_0/I_0) 24:1, solvent THF with 5% v/v water, 0.5 eq. Ag_2SO_4, 10 eq. Cs_2CO_3, the amounts of Ag_2SO_4 and Cs_2CO_3 are given with respect to monomer **5**; [b] Determined with GPC using THF as eluent and calibrated against polystyrene standards.

Kinetic studies and evidence of direct participation of MIDA-boronate monomer in transmetalation. For polymerization kinetic studies, we carried out Ag^+-mediated polymerization of MIDA-boronate monomer **5** in the optimized conditions with M_0/I_0 ratio of 48:1 (entry 14 in Table 1). The polymerization was carried out for the total time of 72 h, and small aliquots were withdrawn at various times during polymerization, the polymer product was precipitated in acetone, and analyzed with GPC. In the first 42 h, the polymer molecular weight (both M_n and M_w) was increasing linearly, while the dispersity stayed constant at $Đ$ 1.2 (Fig. 8). In this stage, the reaction showed pseudo first-order kinetics, with the observed polymerization rate constant k_{polym} 0.040 h^{-1} with respect to M_n. At this point, we carried out some additional experiments to check the accuracy and reproducibility of the kinetic measurements (these experiments are described in detail in the ESI). After 42 h reaction time, the weight average molecular weight M_w continued to increase, albeit at a slower pace, while number average molecular weight M_n remained nearly constant, resulting in significant broadening of the

polymer dispersity in the second stage (Fig. 8). The first stage, up to 42 h polymerization time, showed a linear increase in molecular weight, with constant and narrow dispersity, and therefore reflected a dominating controlled chain-growth polymerization mechanism during this stage. The presence of two distinguished stages in the SCTP process indicated a more complex mechanism than we initially anticipated, and this warranted further studies.

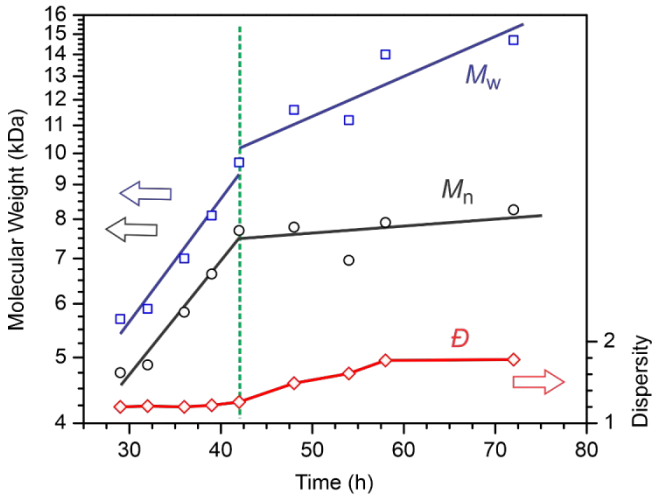

Fig. 8. Kinetic study of Ag^+-mediated SCTP of monomer **5** (M_0/I_0 48:1, reaction conditions are listed in entry 14 in Table 1). The plot illustrates presence of the two stages in the polymerization process, the green dashed line approximately separates the two stages.

Table 3. Monomer to initiator ratio and polymerization time effect on externally initiated SCTP of MIDA boronate monomer **5**. [a]

Entry	M_0/I_0 [b]	Time (h)	Yield (%)	M_n [c] (kDa)	M_w [c] (kDa)	$Đ$ [c]
1	8:1	72	59	5.4	6.6	1.21
2	16:1	72	59	8.1	12.1	1.49
3	24:1	72	42	10.9	15.1	1.39
4	32:1	72	74	18.6	32.4	1.96
5	48:1	72	13	10.3	19.0	1.85
6	64:1	72	2	11.3	24.3	2.15

7	8:1	42	37	4.8	5.6	1.16
8	16:1	42	21	5.1	5.8	1.14
9	24:1	42	42	4.7	5.2	1.11
10	32:1	42	12	4.9	5.4	1.11
11	48:1	42	28	7.9	9.9	1.26
12	64:1	42	18	10.2	19.1	1.88

[a] Reaction conditions: temperature 30 °C, solvent THF with 5% v/v water, 0.5 eq. Ag_2SO_4, 10 eq. Cs_2CO_3, the amounts of Ag_2SO_4 and Cs_2CO_3 are provided with respect to monomer **5**; [b] Monomer **5** to catalytic initiator **3** ratio; [c] Determined with GPC using THF as eluent and calibrated against polystyrene standards.

To further investigate a potential time-dependent mechanistic change, we examined the polymerization dependence on varying M_0/I_0 ratios at two different polymerization times: for 72 h (entries 1-6 in Table 3) and for 42 h (entries 7-12 in Table 3), the latter time representing a first stage dominated by chain-growth polymerization mechanism. All the runs were done with the initial monomer **5** concentration M_0 kept constant (and hence the constant concentrations of Cs_2CO_3 and Ag_2SO_4), and with varying amount of catalytic initiator **3** (I_0). Within the shorter reaction time of 42 h, representing a stage of the controlled chain-growth process, the obtained polymer characteristics were found to be independent of M_0/I_0 up to 32:1 as the M_n remained constant at ~5 kDa with a narrow dispersity $Đ$ not exceeding 1.16. At the same time, the polymer yield showed a generally decreasing trend with the increasing M_0/I_0 ratio. The observed independence of molecular weight on M_0/I_0 ratio along with decreasing polymer yield could be explained by the diminished number of actively growing chains at lower I_0 values (concentration of catalytic initiator **3**). Considering constant monomer concentration (M_0), if each polymer chain grows at the same rate by the chain-growth mechanism (with the pseudo first-order rate constant k_{polym} 0.040 h^{-1}), then all polymers generated within the 42 h polymerization timeframe would be of the same length. With fewer active growing chains at the higher M_0/I_0 ratios, less monomer would be consumed within the limited timeframe leading to lower polymer

yield. At $M_0/I_0 > 32$, the M_n began increasing with broadening dispersity. The loss of control at the higher M_0/I_0 ratios indicated that a second independent mechanistic pathway was likely involved with the monomer that was not able to participate in the principal chain-growth polymerization route.

For the runs with 72 h polymerization time, both M_n (5.4 to 18.6 kDa) and dispersity ($Đ$ 1.21-1.96) were increasing upon M_0/I_0 increase from 8:1 to 32:1, with polymer yield ranging between 42 and 72%. At higher M_0/I_0 ratios (48:1 and 64:1), M_n and polymer yield decreased dramatically with significantly broadened dispersity, although this could have been impacted by low solubility of the higher molecular weight polymer, and difficulties with preparing completely dissolved samples for GPC characterization. The GPC traces showed increasingly bimodal distribution for the polymer product obtained at M_0/I_0 ranging from 16:1 to 64:1 (Fig. S7 in the ESI). This indicated that at these reaction conditions, the polymerization was occurring through two independent mechanistic routes, with the chain-growth route dominating in 42 h runs competing with another route that became particularly prominent at the longer reaction times, or with the large amount of unreacted monomer.

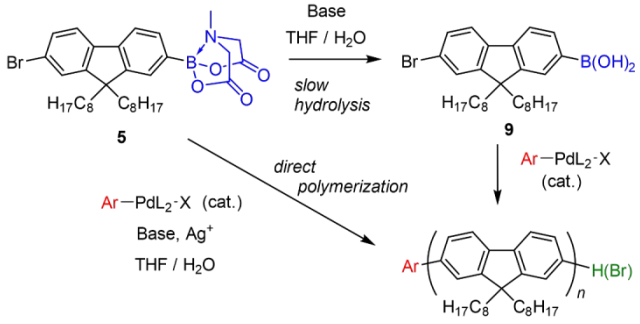

Fig. 9. Conventionally accepted scheme of Suzuki-Miyaura catalyst-transfer polymerization (SCTP) of MIDA-boronate monomer **5** (via intermediate formation of boronic acid **9**), and proposed direct polymerization of MIDA boronate monomer **5** in the conditions of Ag^+-mediated SCTP.

At this point, we kinetically evaluated MIDA-boronate monomer **5** hydrolysis. The accepted rationale behind its use as a monomer in SCTP is that it cannot directly undergo Pd-catalyzed SM cross-coupling but slowly hydrolyzes to release the corresponding boronic acid monomer **9** which then acts

as the actual monomer for chain-growth polymerization (Fig. 9).[48, 75] At the employed polymerization conditions (aqueous THF, milder base), MIDA-boronate is expected to undergo slow hydrolysis (as opposed to fast hydrolysis occurring in the presence of a strong base).[76] We analyzed the hydrolysis kinetics of the monomer **4** in the same reaction conditions as used for polymerization (corresponding to entry 1 in Table 2) but with no added catalytic initiator **3** (Fig. S8 in the ESI). The small aliquots were withdrawn during the reaction and analyzed using ^{1}H NMR spectroscopy. The hydrolysis showed first-order reaction kinetics, with the observed rate constant $k_{\text{hydrolysis}}$ 0.022 h^{-1} (corresponding to the monomer **5** half-life of 33 h). The rate of MIDA-boronate monomer **5** hydrolysis was unaffected by addition of stoichiometric Ag^+. Given that the rate of polymerization within the chain-growth regime (*vide supra*) was roughly twice as fast as the rate of MIDA-boronate hydrolysis, hydrolysis could not be solely responsible for polymerization of **5**, suggesting that the MIDA-boronate monomer **5** must directly participate in the chain-growth polymerization. Interestingly, the hydrolysis half-life roughly matched the time point at around 42 h where the mechanism change (second stage of polymerization) was observed (Fig. 8). From this, one could produce a striking conclusion that, in the conditions of Ag^+-mediated SCTP, MIDA-boronate **5** participated directly in the transmetalation step through the oxo-Pd pathway, while the hydrolysis product, boronic acid **9**, was less efficient in polymerizing through this pathway, and hence was accumulating in the reaction mixture to slowly participate in the second, independent mechanistic route to form the PF polymer. This slower process would become dominating after most of MIDA-boronate monomer **5** has been consumed (both for polymerization and hydrolysis), giving rise to the second, slower stage of polymerization. Although the conclusion about the direct participation of MIDA-boronate compound in SM cross-coupling may seem counterintuitive (as so far MIDA-protected boronic acids have been deemed inert in SM cross-coupling reactions) and has not been observed yet, the possibility of such participation may depend on the reaction conditions. In support of this conjecture, one might recall that another popular class of protected boronic acids, 1,8-diaminonaphthalene boronic acid derivatives [B(dan)], have recently been demonstrated to participate

directly in SM cross-coupling under certain experimental conditions.[77, 78] For MIDA-boronates to directly participate in the transmetalation step via the oxo-Pd pathway, nitrogen has to de-coordinate from the boron center. Yudin *et al.* have recently reported that such a de-coordination could indeed happen in MIDA-boronates with some nucleophiles displacing the amine at tetrasubstituted boron in an S_N2-like fashion.[79, 80] This process may be facilitated by simultaneous coordination of MIDA-boronate to Ag and Pd cations, although specific details of this process are currently unclear and require further special investigation beyond the scope of this work.

In support of the two-stage polymerization mechanism and relative lack of reactivity of the boronic acid monomer **9** during the first polymerization stage, one could use the experimentally measurable composition of the reaction mixture at the end of the first stage. If Ag^+-mediated chain-growth SCTP proceeds through direct participation of MIDA-boronate monomer **5**, whereas independently occurring hydrolysis produces relatively unreactive (under these specific reaction conditions) boronic acid **9**, and assuming that these two parallel processes follow pseudo first-order kinetic laws (with the corresponding rate constants k_{polym} 0.040 h^{-1} and $k_{hydrolysis}$ 0.022 h^{-1}), one could calculate that, after 42 h reaction time, the reaction mixture would contain 60% of PF polymer, 33% of boronic acid **9**, and 7% of unreacted MIDA-boronate monomer **5**. Mass balance analysis of the composition of the reaction mixture after 42 h polymerization time (in the conditions of entry 9 in Table 3) was carried out via precipitation of the reaction mixture in acetone to determine the amount of precipitated polymer, and analyzing the composition of mother liquor by ^1H NMR to determine the amounts of boronic acid **9** and MIDA-boronate monomer **5**. The analysis produced 49% of the polymer, 39% of boronic acid **9**, and 12% of unreacted MIDA boronate monomer **5**. The obtained numbers qualitatively matched the calculated distribution; the discrepancy could be due to experimental errors with experimental quantitation of the reaction mixture composition (e.g. due to incomplete precipitation of PF polymer), but also could be related to undesired chain termination processes occurring later in polymerization. Such premature chain termination was previously suggested by McCullough *et al.* to

explain curved semilogarithmic kinetic plots observed in a case of Ni^{II}-catalyzed Kumada CTP of a fluorene Grignard monomer, and was ascribed to aggregation of the higher molecular weight PF polymer chains hindering further polymerization.[81] Noonan *et al.* have also noticed a similarly curved semilogarithmic kinetic plot in the Ni^{II}-catalyzed SCTP of a 3-hexylthiophene pinacol-boronate monomer (similar to the monomer **1** in Fig. 1) although no mechanistic explanation for their observation was provided.[82] Whereas similar premature chain termination might have played some role in leveling off the kinetic plots in the case of Ag^+-mediated polymerization of MIDA-boronate monomer **5**, the significant accumulation of boronic acid monomer **9** cannot be accounted for by solely considering this process, and requires invoking a proposed two-stage polymerization scheme.

The competition between direct polymerization of MIDA-boronate monomer and its hydrolysis to (relatively unreactive) boronic acid **9** could explain why the polymer yield in Ag^+-mediated SCTP was typically around 30 to 50%. The yield would drop even further at the higher M_0/I_0 ratios (as presented in Table 3) as more MIDA-boronate monomer **5** would hydrolyze to boronic acid **10** and thus become unavailable for direct polymerization.[83]

Fig. 10 shows monitoring of the composition of the reaction mixture for Ag^+-mediated SCTP of monomer **5** (in the experimental conditions of entry 9 in Table 3) using ^{11}B NMR spectroscopy. Although ^{11}B NMR spectra could not be used for quantitative analysis of the reaction mixture, it could reveal the boron-containing species present at various times during the polymerization. Before addition of catalytic initiator **3** to start the polymerization, only a single broad ^{11}B signal of MIDA-boronate monomer **5** was observed at 12.1 ppm. In addition to this signal, after 24 h of polymerization, a high intensity broad signal at 30.4 ppm from boronic acid **9** and an additional peak at 20.1 ppm from boric acid appeared. After 48 h of polymerization, the intensity of MIDA-boronate signal substantially diminished while the signal from boronic acid **9** remained intense, along with the boric acid peak. Finally, after 96 h polymerization time, all signals nearly vanished except for the peak from boric acid. These observations qualitatively support the direct involvement of MIDA-boronate monomer **5** in Ag^+-

mediated SCTP process, while boronic acid **9** that was formed as a result of slow hydrolysis of **5** remained much less reactive in the polymerization process and was accumulating during the first stage of the polymerization.

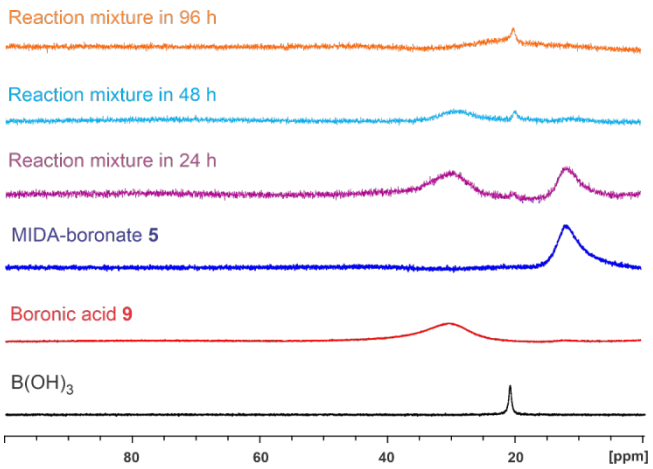

Fig. 10. Monitoring of Ag^+-mediated SCTP of MIDA-boronate monomer **5** using ^{11}B NMR. The polymerization was carried out in the reaction conditions of entry 9 in Table 3, and each spectrum was acquired from a small aliquot withdrawn from the reaction. Reference ^{11}B NMR spectra of boric acid and boronic acid **9** were acquired in the same conditions as used for monitoring the polymerization.

Kinetic analysis of the small-molecule cross-coupling: further evidence of direct coupling of MIDA-boronates. The intriguing conclusion about the direct participation of MIDA-boronate **5** in SCTP process prompted us to investigate if the same phenomenon could be observed in the analogous case of small-molecule cross-coupling of MIDA-boronate **10** and catalytic initiator **3** (Fig. 11), both in the Ag^+-mediated conditions and without added Ag^+. During the reaction, small aliquots of the reaction mixture were withdrawn at specific time intervals and analyzed using ^1H NMR to determine the fractional amount of the MIDA-boronate **10** and the coupling product **11** (further details of this experiment are provided in the ESI). The resulting kinetic plot is presented in Fig. 12. One can notice a substantial difference between the observed cross-coupling rate constants for the Ag^+-mediated cross-coupling vs. the reaction carried out in Ag^+-free conditions (0.035 h^{-1} vs. 0.013 h^{-1}). We also studied

kinetics of MIDA-boronate **11** hydrolysis carried out in the same reaction conditions (Fig. 12). The obtained hydrolysis rate constants did not change in response to added Ag^+ ($k_{hydrolysis}$ 0.021 h^{-1} both in the Ag^+-mediated and Ag^+-free reaction conditions). As with the polymerization of monomer **5**, the observed cross-coupling rate constant in Ag^+-mediated conditions was substantially higher than the corresponding hydrolysis rate of MIDA-boronate **10** thus pointing on the possibility of direct participation of the MIDA-boronate **10** in the cross-coupling process. On the other hand, the observed cross-coupling rate constant for the reaction in Ag^+-free conditions (0.013 h^{-1}) was lower than the corresponding hydrolysis rate constant (0.021 h^{-1}) indicating that transmetalation of the corresponding boronic acid (rather than MIDA-boronate hydrolysis) seemed to be the rate-determining step in the Ag^+-free coupling conditions. Therefore, the small-molecule cross-coupling kinetic data also revealed direct participation of MIDA-boronate in Ag^+-mediated conditions, thus providing an additional support for the same phenomenon observed for the Ag^+-mediated SCTP process.

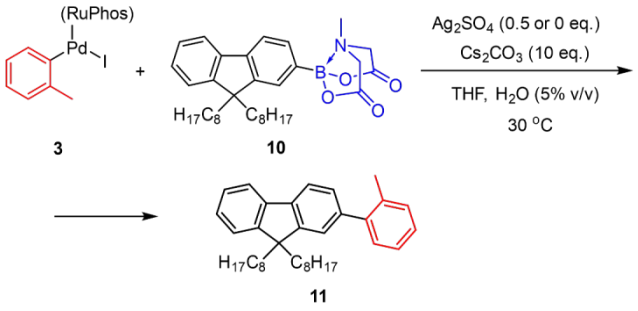

Fig. 11. Cross-coupling between Pd^{II} catalytic initiator **3** and MIDA-boronate **10**.

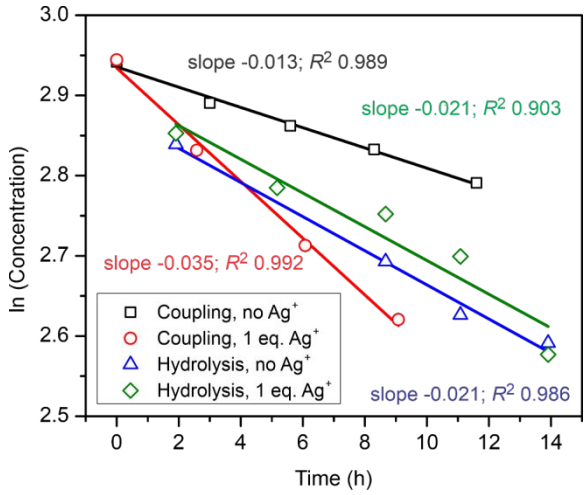

Fig. 12. Semilogarithmic kinetic plots for the small-molecule cross-coupling reaction in Fig. 11 and hydrolysis of MIDA-boronate **10**. The concentration refers to MIDA-boronate **10** which participated in cross-coupling reaction (hence the negative slope). The reaction conditions are indicated in Fig. 11; "no Ag^+" refers to Ag^+-free reaction conditions, and "1 eq. Ag^+" refers to Ag^+-mediated conditions.

The interplay between two transmetalation pathways. The experiments described above demonstrated that MIDA-boronate **5** must have reacted directly in the transmetalation step of Ag^+-mediated SCTP. In addition, we found that boronic acid **9** that was formed as a result of the slow hydrolysis of **5** could also participate in polymerization, albeit at a noticeably slower rate. The contribution of the polymer product from the second route (i.e. boronic acid **9** polymerization) was becoming more prominent when polymerization was allowed to run for longer than a 42 h period, e.g. in the 72 h polymerization experiments describe above. In the longer runs, due to consumption of the MIDA-boronate monomer **5** in the first 42 h, the contribution of the route linked to the direct involvement of **5** in oxo-Pd transmetalation pathway would diminish, and additional polymer would be furnished via polymerization of the boronic acid **9** monomer occurring through the second route. Initially, we hypothesized that the second route involved step-growth polymerization (based on the increasing dispersity of the produced polymer), however MALDI-TOF analysis of the polymers revealed that even at longer polymerization times the dominating composition of the polymer chains

were Tol–$(PF)_n$–Br and Tol–$(PF)_n$–H, indicating that all these chains resulted from the controlled chain-growth process started by the catalytic initiator **3**.

Table 4. Externally initiated SCTP of various monomers. [a]

Entry	Monomer	H_2O (% v/v)	Base (eq.)	Ag_2SO_4 (eq.)	Yield (%)	M_n [b] (kDa)	M_w [b] (kDa)	$Đ$ [b]
1	**5**	0	Cs_2CO_3 (10)	0.5	<5	–	–	–
2	**5**	3	Cs_2CO_3 (10)	0.5	13	3.8	4.3	1.14
3	**5**	5	Cs_2CO_3 (10)	0.5	34	6.1	7.6	1.24
4	**5**	8	Cs_2CO_3 (10)	0.5	44	6.2	7.5	1.20
5	**5**	10	Cs_2CO_3 (10)	0.5	55	9.5	12.2	1.28
6	**5**	13	Cs_2CO_3 (10)	0.5	77	13.6	20.8	1.53
7	**5**	15	Cs_2CO_3 (10)	0.5	91	13.2	21.0	1.59
8	**5**	10	Cs_2CO_3 (10)	0.5	49	8.8	11.3	1.28
9	**5**	10	Cs_2CO_3 (10)	1.0	37	6.3	7.6	1.21
10	**5**	10	Cs_2CO_3 (10)	1.5	27	4.8	5.3	1.16
11 [c]	**13**	0	no base	0	57	5.7	7.0	1.22
12 [c]	**13**	10	no base	0	60	7.5	10.1	1.35
13 [c]	**13**	10	no base	0.5	72	9.1	14.2	1.56
14 [c]	**13**	10	Cs_2CO_3 (1)	0	66	8.6	12.3	1.43
15 [c]	**13**	10	Cs_2CO_3 (1)	0.5	71	10.2	17.2	1.68
16	**9**	5	Cs_2CO_3 (10)	0	9	8.9	11.2	1.26
17	**9**	5	Cs_2CO_3 (10)	0.5	23	11.0	23.6	1.96
18	**9**	5	Cs_2CO_3 (10)	1.5	25	13.3	28.7	2.15
19	**1**	5	Cs_2CO_3 (10)	0	42	4.9	5.4	1.09
20	**1**	5	Cs_2CO_3 (10)	0.5	53	4.4	4.8	1.09

[a] Reaction conditions: temperature 30 °C, reaction time 42 h (except entries 11-15 where reaction time was 4 h), monomer to initiator **3** ratio (M_0/I_0) 24:1, solvent THF with indicated percentage of water; [b]

Determined with GPC using THF as eluent and calibrated against polystyrene standards; [c] Reaction time 4 h.

To investigate the relative contribution of the two routes, we carried out Ag^+-mediated polymerization of MIDA-boronate monomer **5** in the conditions of varying water concentration with the M_0/I_0 ratio at 24:1 and polymerization time of 42 h (entries 1-7 in Table 4). As expected, carrying out the reaction in the absence of water resulted in no polymerization (entry 1 in Table 4). Gradually increasing the water content resulted in gradually increasing yield of the polymer product (up to 91% for 15% v/v H_2O) with increasing M_n, but also in broadening dispersity ($Đ$ 1.59 for 15% v/v H_2O). MALDI-TOF data for the polymers revealed stark differences in their chain composition. The polymer obtained in the conditions of 5% v/v H_2O showed a uniform monomodal distribution, with dominating Tol–$(PF)_n$–H chain composition (Fig. 13a). The polymer obtained in the conditions of 10% v/v H_2O showed a bimodal distribution, with the larger molecular weight component characterized by predominant Tol–$(PF)_n$–H chain composition, whereas the smaller molecular weight component was characterized by equally dominant Tol–$(PF)_n$–H and Tol–$(PF)_n$–Br compositions (Fig. 13b). The bimodal distribution became even more pronounced in the polymer obtained in the 15% v/v H_2O conditions (Fig. 13c); the bimodality was even noticeable in the GPC trace for this polymer sample (Fig. S9 in the ESI). It should be noted that the higher molecular weight component (showing predominantly Tol–$(PF)_n$–H chain composition) was gradually shifting toward the higher molecular weight with increasing water content during polymerization, whereas the lower molecular weight component was much less affected. Since the lower molecular weight component was not present in the polymer obtained in the conditions of 5% v/v H_2O, and since we found from the above studies that the polymer obtained in such conditions would originate from the polymerization route involving direct MIDA-boronate participation in transmetalation via the oxo-Pd pathway, we could assign the higher molecular weight distribution as resulting from the route corresponding to the more efficient oxo-Pd pathway.

This distribution was characteristically distinguished by the Tol–$(PF)_n$–H chain composition. Therefore, the lower molecular weight distribution could be the one resulting from the second chain-growth route; this distribution's main structural feature was an approximately equal abundance of the chains with Tol–$(PF)_n$–H and Tol–$(PF)_n$–Br compositions.

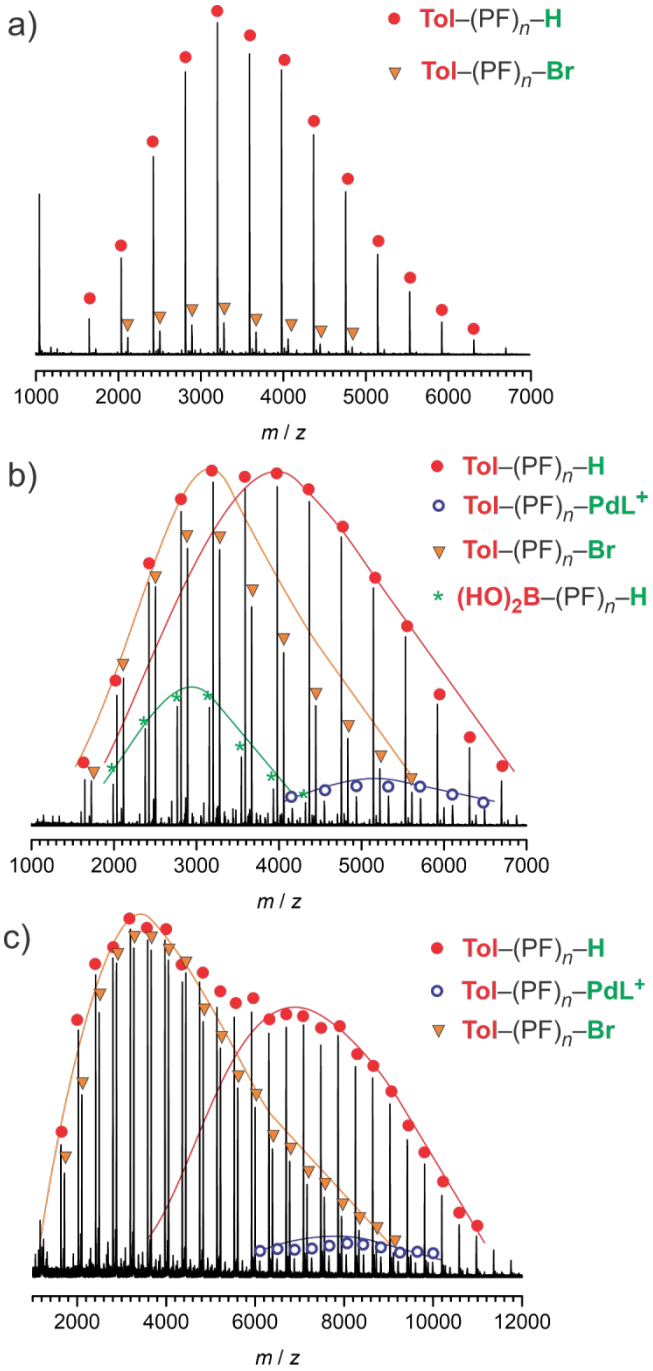

Fig. 13. MALDI-TOF data for the PF polymer produced in Ag^+-mediated SCTP in the conditions of varying water content: a) 5% v/v H_2O (entry 3 in Table 4), b) 10% v/v H_2O (entry 5 in Table 4), and c) 15% v/v H_2O (entry 7 in Table 4). The chain composition corresponding to specific peaks is marked with colored symbols, L is RuPhos; the outline of different peak distributions is approximate.

What was the second, less efficient polymerization route? It was apparent that this second route should likely involve boronic acid monomer **9** produced as a result of MIDA-boronate **5** hydrolysis. With increasing fraction of water in the polymerization medium, both the rate of hydrolysis and the rate of the MIDA-boronate polymerization through the oxo-Pd transmetalation pathway must increase. Indeed, kinetic studies of the hydrolysis of **5** in the 10% v/v H_2O reaction conditions (Fig. S8 in the ESI) yielded the hydrolysis rate constant $k_{hydrolysis}$ 0.087 h^{-1}, which was nearly 4 times higher than the corresponding rate constant in 5% v/v H_2O conditions (*vide supra*). At the same time, the rate of polymerization occurring by the first route (i.e. via oxo-Pd transmetalation pathway) also increased by more than 2 times (pseudo first-order rate constant k_{polym} 0.088 h^{-1}, Fig. S10 in the ESI). The higher k_{polym} allowed for more MIDA-boronate monomer **5** to be directly consumed via the first route involving oxo-Pd transmetalation, and this could explain the gradual shift of the corresponding MALDI-TOF distribution towards higher molecular weight, and overall increase in M_n in the higher water content polymerization conditions. At the same time, faster hydrolysis rate of **5** produced more boronic acid **9** monomer available for the polymerization by the second, less efficient, independent route, resulting in increasing fraction of the corresponding lower molecular weight distribution in the MALDI-TOF data. This second route was noticeably hindered in the Ag^+-mediated SCTP process which heavily favored the more efficient route through oxo-Pd transmetalation. From the inefficiency of the second route in the polymerization conditions favoring the oxo-Pd transmetalation pathway, it would be logical to assume that the second route must involve the boronate transmetalation pathway.

The proposed mechanism of polymerization of **5** involving interplay between the two routes is shown in Fig. 14. In this mechanism, the principal catalytic cycle involves the oxo-Pd transmetalation

pathway: the ArPd(L)–Br oxidative addition intermediate ***I*** undergoes anion exchange (facilitated by the presence of Ag^+) to form oxo-Pd intermediate ***II***. This intermediate undergoes direct transmetalation with MIDA-boronate monomer **5** to form the intermediate ***III***. Reductive elimination in ***III*** forms the associated Pd^0 π-complex ***IVa***, where intramolecular catalyst transfer step furnishes π-complex ***IVb***, which undergoes oxidative addition to the terminal C–Br bond to produce the intermediate ***I***. The intermediate ***I*** remains the resting state of the polymerization, therefore upon quenching the reaction mixture with HCl it produces the product polymer with Tol–$(PF)_n$–H chain composition (and upon incomplete quenching also leaves behind Tol–$(PF)_n$–Pd(L)Br chains, *vide supra*). Since the polymerization rate increases with increasing amount of water in the reaction medium, as well as exhibits pseudo first-order kinetics with respect to monomer **5**, both the formation of oxo-Pd intermediate ***II*** and transmetalation to form intermediate ***III*** must be comparably slow steps in the mechanism. Nevertheless, presence of Ag^+ in the Ag^+-mediated conditions likely accelerates both the formation of oxo-Pd intermediate ***II*** and subsequent transmetalation with monomer **5**, resulting in overall increasing efficiency of this polymerization route.

Since slow hydrolysis of MIDA boronate monomer **5** (bottom line in the mechanism in Fig. 14) ensues immediately upon mixing together the reactants, some small amount of boronic acid **9** becomes available at the start of polymerization, which is converted by the base to the corresponding "ate" boronate **12**, and it can react with the ArPd(L)–Br complex ***I*** in the boronate transmetalation pathway. Although both transmetalation pathways can occur simultaneously leading to the same diarylpalladium complex ***III***, in the conditions of Ag^+-mediated SCTP which heavily favor oxo-Pd pathway, in the early stage of polymerization the route through boronate pathway remains inefficient, and most polymer is produced through the route involving direct MIDA-boronate **5** transmetalation via the oxo-Pd pathway. In addition to the inefficient boronate **12** transmetalation via the boronate pathway, transmetalation through the oxo-Pd pathway involving boronic acid **9** also appears hindered. Although, in principle, the reaction of boronic acid **9** with oxo-Pd intermediate ***II*** could contribute to the overall reactivity through

the oxo-Pd transmetallation pathway, the experimentally observed accumulation of the boronic acid monomer **9** and faster reaction of MIDA-boronate monomer **5** in the first stage of polymerization in Ag^+-mediated conditions strongly point on the suppression of boronic acid reactivity in both transmetalation pathways. It is possible that the large excess of base (10 eq. Cs_2CO_3 with respect to monomer **5**) favors formation of the "ate" boronate **12** which can no longer react through the oxo-Pd transmetalation pathway. This issue requires a further detailed investigation which is beyond the scope of this work.

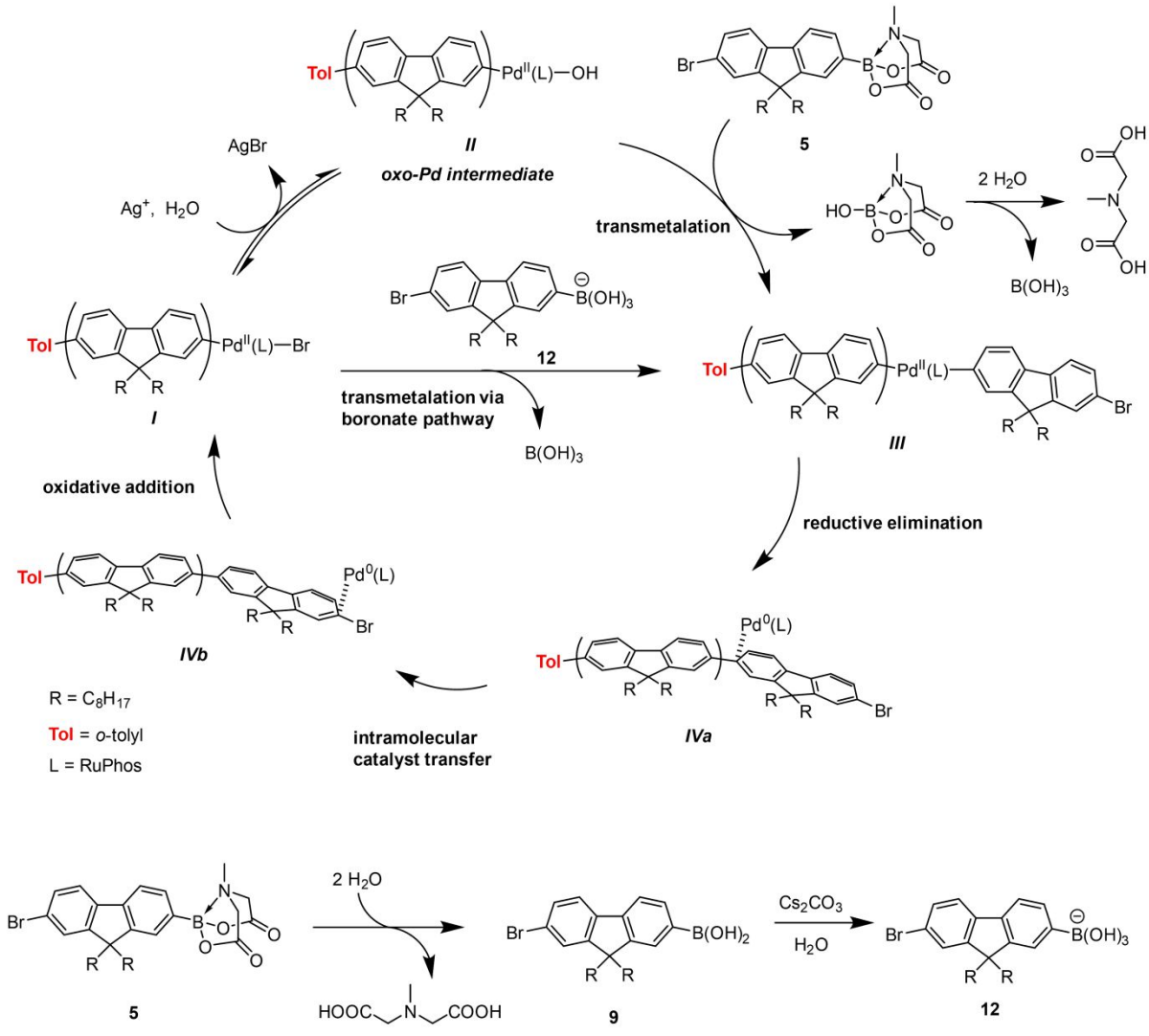

Fig. 14. Proposed mechanism of the Ag^+-mediated polymerization of MIDA boronate monomer **5** showing competition between oxo-Pd and boronate transmetalation pathways.

In the intermediate stage of the polymerization, when the amount of unreacted MIDA-boronate **5** decreases and the concentration of boronic acid **9** increases, contribution of the boronate transmetalation pathway with "ate" boronate **12** becomes more substantial. The competition of the two pathways starts forming two separate molecular weight distributions (which become especially well-separated upon increasing both the rates of hydrolysis of **5** and polymerization of **5** via the oxo-Pd route in the conditions with higher water content). Finally, in the late stage of the polymerization, only a slower process involving boronate transmetalation pathway with the "ate" boronate **12** can occur. It is noteworthy that the lower molecular weight distribution is characterized by a significant contribution of Tol–$(PF)_n$–Br chain composition (Fig. 13b, c). This could happen if, upon acid quenching, the polymer was existing as a Pd^0 associated π-complex ***IVa*** or ***IVb*** (Fig. 14), indicating that the π-complex was a resting state for polymerization through the route involving the boronate transmetalation pathway. While it is not surprising for the two catalytic routes to have different resting states, in this case the two routes are interconnected as they involve the same intermediate complexes ***I*** and ***III***. However, in the early stage of polymerization, the route involving direct MIDA-boronate transmetalation via the oxo-Pd pathway dominates over the less efficient route via the boronate transmetalation pathway, and in the late stage of polymerization, due to the absence of MIDA-boronate monomer, the former route is suppressed and polymerization can only proceed through the route involving the boronate transmetalation pathway. Thus, each of the two routes operates nearly exclusively at early and late stages of polymerization, while both of them competitively operate during the intermediate stage of the polymerization process.

One question remains to be discussed: what is the role of Ag^+? Undoubtedly, its presence in the reaction mixture enforces the oxo-Pd transmetalation pathway by shifting the equilibrium toward Ar–Pd(L)–OH intermediate ***II***, and Ag^+ might also activate MIDA-boronate monomer to react directly in transmetalation step. On the other hand, the presence of Ag^+ in the reaction mixture might hinder

boronic acid monomer **9**'s ability to participate in the transmetalation step, as could be judged from the low reactivity and accumulation of this compound in the reaction mixture during polymerization. Indeed, increasing the amount of Ag^+ from 1 to 2 and then to 3 equivalents in the conditions of 10% v/v H_2O (entries 8-10 in Table 4) resulted in suppression of the lower molecular weight polymer component corresponding to the boronate transmetalation pathway as was revealed in MALDI-TOF experiments (Fig. S12 in the ESI). With 3 equivalents of Ag^+, the low molecular weight component essentially did not form (Fig. S12c). At the same time, excess Ag^+ did not affect the rate of polymerization through direct MIDA-boronate transmetalation via oxo-Pd pathway (the polymerization rate constant k_{polym} of **5** at 10% v/v H_2O in the presence of 2 eq. of Ag^+ was found to be 0.083 h^{-1} (Fig. S11 in the ESI) compared to 0.088 h^{-1} for polymerization in the same conditions in the presence of 1 eq. Ag^+). Thus, increasing Ag^+ concentration in the reaction mixture further suppressed the boronate pathway, allowing the polymerization to occur only through the route involving the oxo-Pd transmetalation pathway. The origin of this hindering effect is not clear at this point; whereas it might be related to some interactions between excess Ag^+ and a negatively charged "ate" boronate complex **12**, further studies are required to understand this phenomenon.

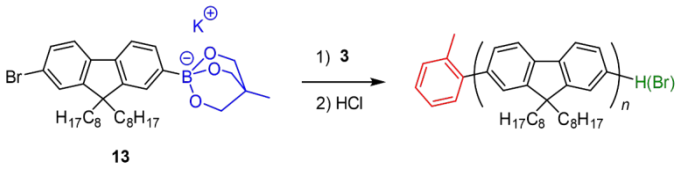

Fig. 15. Externally-initiated polymerization of triolboronate monomer **13**. Specific reaction conditions are given in entries 11-15 in Table 4.

The role of the boronate transmetalation pathway. Whereas the studies described above pointed on domination of the oxo-Pd transmetalation pathway in the case of Ag^+-mediated SCTP of MIDA-boronate monomer **5**, they also indicated that in the same conditions the more common boronic

acid monomer **9** undergoes SCTP via the boronate transmetalation pathway (which is suppressed in the Ag^+-mediated conditions). This brings about a more general question of which transmetalation pathway dominates in the more conventional SCTP conditions (i.e. in the absence of Ag^+). To study this, we carried out polymerization of the cyclic triolboronate monomer **13** (Fig. 15).[84] The cyclic triolboronates are essentially pre-formed boronate "ate" complexes, and they are convenient SM cross-coupling partners as they efficiently cross-couple with aryl halides in anhydrous conditions with no need for additional base, apparently via the boronate transmetalation pathway.[85]

Polymerization of **13** with catalytic initiator **3** (with M_0/I_0 ratio of 24:1) in anhydrous THF without added base and Ag^+ proceeded smoothly and yielded polymer with M_n 5.7 kDa and narrow dispersity $Đ$ 1.22 (entry 11 in Table 4). This result reflected a cleanly occurring chain-growth controlled SCTP process. Adding water to the polymerization medium produced a polymer with higher molecular weight, M_n 7.5 kDa, but with a somewhat higher dispersity $Đ$ 1.35 (entry 12 in Table 4). Adding base did not significantly affect the polymerization outcome (entry 14 in Table 4). In contrast, carrying out the polymerization in the presence of 1 eq. of Ag^+ produced a polymer of higher molecular weight but also with broader dispersity indicative of a bimodal distribution (entries 13 and 15 in Table 4). MALDI-TOF analysis of the polymer samples revealed that in the absence of water, base and Ag^+, the resulting polymer had a uniform chain distribution, with predominantly Tol–$(PF)_n$–H chain composition (Fig. S13a in the ESI). Adding water resulted in a slight appearance of the second, higher molecular weight distribution with Tol–$(PF)_n$–H chain composition, whereas the main distribution now included both the Tol–$(PF)_n$–H and Tol–$(PF)_n$–Br end groups (Fig. S13b). Finally, with added Ag^+, the presence of the higher molecular weight distribution (with Tol–$(PF)_n$–H end groups) was evident, whereas the lower molecular weight distribution featured heavy presence of Tol–$(PF)_n$–Br chain composition (Fig. S13c). The increasing content of Tol–$(PF)_n$–Br chains was consistent with the suppressed boronate transmetalation pathway (particularly evident in the Ag^+-mediated polymerization conditions), and the appearance of the higher molecular weight distribution was indicative of the oxo-Pd transmetalation

pathway becoming more prominent with added water, and especially with added Ag^+. Thus, one should conclude that, in the absence of Ag^+, SCTP of the cyclic triolboronate monomer was presumably occurring through the boronate transmetalation pathway, whereas addition of Ag^+ resulted in partial suppression of that pathway while diverging the reaction toward the oxo-Pd transmetalation pathway.

The possibility to alter the dominating transmetalation pathway during polymerization was observed in the case of SCTP with boronic acid monomer **9** (entries 16-18 in Table 4). In the absence of added Ag^+ (entry 16) the reaction proceeded cleanly (although with low polymer yield) presumably via boronate transmetalation pathway (or possibly through a combination of comparably efficient boronate and oxo-Pd pathways) and yielded a characteristic single narrow distribution in MALDI-TOF data with the Tol–$(PF)_n$–H dominating chain composition (Fig. S14a in the ESI). Carrying out polymerization in the conditions with added 1 eq. of Ag^+ (entry 17) produced what appeared to be a bimodal distribution in MALDI-TOF data with both distributions still possessing predominant Tol–$(PF)_n$–H chain composition (Fig. S14b): the original intense distribution shifted to a lower molecular weight, whereas a second less intense distribution appeared as a pronounced shoulder at a higher molecular weight (resulting in an overall high dispersity index $Đ$ 1.96). The polymerization outcome did not significantly change in the conditions with 3 eq. of Ag^+ (entry 18 in Table 4, and Fig. S14c). The results of these experiments could be rationalized considering that (1) the boronate transmetalation pathway would be hindered in the Ag^+-mediated conditions which favor the oxo-Pd transmetalation pathway, and (2) the boronic acid monomer **9** displays low reactivity toward oxo-Pd transmetalation pathway in the Ag^+-mediated conditions.[86] Therefore, in Ag^+-mediated conditions, the route involving boronate transmetalation pathway still remained dominating, albeit less efficient (hence the shift of the main MALDI-TOF distribution toward the lower molecular weight), whereas the more efficient oxo-Pd transmetalation route (leading to the higher molecular weight distribution) was contributing less substantially due to the diminished reactivity of the boronic acid monomer **9** in Ag^+-mediated oxo-Pd transmetalation route.

Conclusions

Suzuki-Miyaura catalyst-transfer polymerization (SCTP) of MIDA-boronate monomers stands as a promising approach toward controlled preparation of various CPs. Further expansion and development of practical applications of this method will hinge on unified mechanistic understanding of both the entire process and the particular steps involved in the catalytic cycle. In our work, we introduced, for the first time, Ag^+-mediated SCTP and demonstrated that presence of Ag^+ shifted a key transmetalation step toward the oxo-Pd pathway, leading to direct participation of MIDA-boronates in the transmetalation step and hence in the polymerization process. The direct participation of MIDA-boronates in Suzuki-Miyaura cross-coupling has not been envisaged previously and could enable new interesting possibilities to control this reaction both for small-molecule and macromolecular syntheses. On the other hand, boronic acid monomers likely undergo transmetalation through an alternative boronate pathway, although they may be forced to react, albeit with lower efficiency, via the oxo-Pd transmetalation pathway in the Ag^+-mediated conditions. The interplay between the two transmetalation pathways which are both involved in the polymerization, and the opportunity to selectively enhance one of them not only improves mechanistic understanding of SCTP process but also provides a previously unexplored possibility to increase reactivity and gain more effective control over the polymerization to obtain structurally better-defined conjugated polymers. This possibility would be particularly valuable for the arene monomers that do not show particularly high efficiency in SCTP (e.g. the fluorenyl monomers used in this work). The improvement observed in Ag^+-mediated SCTP, however, may be less noticeable in the situations involving monomers that are highly efficient in SCTP process, such as thienyl monomers (e.g. 3-hexylthiophene monomer **1**). Indeed, polymerization of MIDA-boronate monomer **1** in SCTP conditions with catalytic initiator **3** resulted in formation of P3HT polymers with similar molecular weight and narrow dispersity both in the absence and presence of added Ag_2SO_4 (entries 19 and 20 in Table 4). The MALDI-TOF data analysis (Fig. S15 in the ESI) indicated that both

polymers consisted of structurally homogeneous molecular chains with uniform composition (Tol–P3HT–H) which indicated a well-controlled catalyst-transfer polymerization process which was highly efficient even without added Ag^+ and hence could not benefit from using the Ag^+-mediated conditions. Clearly, our targets are the monomers that are less efficient in SCTP process which can benefit from the possibility of further reaction improvement achieved in Ag^+-mediated conditions. We foresee that our mechanistic study will act as a platform for further research on SCTP – an important controlled polymerization process toward various classes of CPs.

Data Availability. Detailed synthetic and experimental procedures, and additional data and figures for this article have been included in the ESI.

Conflicts of Interest

The authors declare no conflicts of interest.

Acknowledgements. This research was supported by the U.S. National Science Foundation (NSF) under the grant CHE-2004117. Purchase of the NMR spectrometer used to obtain results included in this publication was supported by the NSF under the MRI award CHE-2117776. We thank Dr. Fabrizio Donnarumma (Louisiana State University) for assistance with acquiring MALDI-TOF data.

References:

(1) C. S. Fischer, M. C. Baier and S. Mecking, *J. Am. Chem. Soc.* 2013, **135**, 1148-1154.

(2) M. J. Robb, D. Montarnal, N. D. Eisenmenger, S.-Y. Ku, M. L. Chabinyc and C. J. Hawker, *Macromolecules* 2013, **46**, 6431-6438.

(3) C. Ego, D. Marsitzky, S. Becker, J. Zhang, A. C. Grimsdale, K. Müllen, J. D. MacKenzie, C. Silva and R. H. Friend, *J. Am. Chem. Soc.* 2003, **125**, 437-443.

(4) K. Becker and J. M. Lupton, *J. Am. Chem. Soc.* 2006, **128**, 6468-6479.

(5) M. C. Baier, J. Huber and S. Mecking, *J. Am. Chem. Soc.* 2009, **131**, 14267-14273.

(6) A. Gregory and M. H. Stenzel, *Prog. Polym. Sci.* 2012, **37**, 38-105.

(7) M. Chen, M. Zhong and J. A. Johnson, *Chem. Rev.* 2016, **116**, 10167-10211.

(8) J.-F. Lutz, *Polym. Chem.* 2010, **1**, 55-62.

(9) J.-F. Lutz, J.-M. Lehn, E. W. Meijer and K. Matyjaszewski, *Nat. Rev. Mater.* 2016, **1**, 16024.

(10) C. Boyer, N. A. Corrigan, K. Jung, D. Nguyen, T.-K. Nguyen, N. N. M. Adnan, S. Oliver, S. Shanmugam and J. Yeow, *Chem. Rev.* 2016, **116**, 1803-1949.

(11) J. P. Lutz, M. D. Hannigan and A. J. McNeil, *Coord. Chem. Rev.* 2018, **376**, 225-247.

(12) Z. J. Bryan and A. J. McNeil, *Macromolecules* 2013, **46**, 8395-8405.

(13) A. Kiriy, V. Senkovskyy and M. Sommer, *Macromol. Rapid Commun.* 2011, **32**, 1503-1517.

(14) K. Okamoto and C. K. Luscombe, *Polym. Chem.* 2011, **2**, 2424-2434.

(15) R. Miyakoshi, A. Yokoyama and T. Yokozawa, *J. Polym. Sci., Part A: Polym. Chem.* 2008, **46**, 753-765.

(16) A. K. Leone, E. A. Mueller and A. J. McNeil, *J. Am. Chem. Soc.* 2018, **140**, 15126-15139.

(17) E. E. Sheina, J. Liu, M. C. Iovu, D. W. Laird and R. D. McCullough, *Macromolecules* 2004, **37**, 3526-3528.

(18) M. C. Iovu, E. E. Sheina, R. R. Gil and R. D. McCullough, *Macromolecules* 2005, **38**, 8649-8656.

(19) A. Yokoyama, R. Miyakoshi and T. Yokozawa, *Macromolecules* 2004, **37**, 1169-1171.

(20) R. Miyakoshi, A. Yokoyama and T. Yokozawa, *J. Am. Chem. Soc.* 2005, **127**, 17542-17547.

(21) W. He, B. O. Patrick and P. Kennepohl, *Nat. Commun.* 2018, **9**, 3866.

(22) E. L. Lanni and A. J. McNeil, *J. Am. Chem. Soc.* 2009, **131**, 16573-16579.

(23) N. Doubina, M. Stoddard, H. A. Bronstein, A. K.-Y. Jen and C. K. Luscombe, *Macromol. Chem. Phys.* 2009, **210**, 1966-1972.

(24) N. Doubina, A. Ho, A. K.-Y. Jen and C. K. Luscombe, *Macromolecules* 2009, **42**, 7670-7677.

(25) E. L. Lanni and A. J. McNeil, *Macromolecules* 2010, **43**, 8039-8044.

(26) M. A. Baker, C.-H. Tsai and K. J. T. Noonan, *Chem. Eur. J.* 2018, **24**, 13078-13088.

(27) I. P. Beletskaya, F. Alonso and V. Tyurin, *Coord. Chem. Rev.* 2019, **385**, 137-173.

(28) R. Martin and S. L. Buchwald, *Acc. Chem. Res.* 2008, **41**, 1461-1473.

(29) C. C. C. Johansson Seechurn, M. O. Kitching, T. J. Colacot and V. Snieckus, *Angew. Chem. Int. Ed.* 2012, **51**, 5062-5085.

(30) M. V. Bautista, A. J. Varni, J. Ayuso-Carrillo, M. C. Carson and K. J. T. Noonan, *Polym. Chem.* 2021, **12**, 1404-1414.

(31) A. Yokoyama, H. Suzuki, Y. Kubota, K. Ohuchi, H. Higashimura and T. Yokozawa, *J. Am. Chem. Soc.* 2007, **129**, 7236-7237.

(32) T. Yokozawa, H. Kohno, Y. Ohta and A. Yokoyama, *Macromolecules* 2010, **43**, 7095-7100.

(33) T. Beryozkina, K. Boyko, N. Khanduyeva, V. Senkovskyy, M. Horecha, U. Oertel, F. Simon, M. Stamm and A. Kiriy, *Angew. Chem. Int. Ed.* 2009, **48**, 2695-2698.

(34) E. Elmalem, A. Kiriy and W. T. S. Huck, *Macromolecules* 2011, **44**, 9057-9061.

(35) H.-H. Zhang, W. Peng, J. Dong and Q.-S. Hu, *ACS Macro Lett.* 2016, **5**, 656-660.

(36) A. Sui, X. Shi, H. Tian, Y. Geng and F. Wang, *Polym. Chem.* 2014, **5**, 7072-7080.

(37) T. Yokozawa, R. Suzuki, M. Nojima, Y. Ohta and A. Yokoyama, *Macromol. Rapid Commun.* 2011, **32**, 801-806.

(38) H.-H. Zhang, C.-H. Xing and Q.-S. Hu, *J. Am. Chem. Soc.* 2012, **134**, 13156-13159.

(39) K. Kosaka, T. Uchida, K. Mikami, Y. Ohta and T. Yokozawa, *Macromolecules* 2018, **51**, 364-369.

(40) K. Mikami, M. Nojima, Y. Masumoto, Y. Mizukoshi, R. Takita, T. Yokozawa and M. Uchiyama, *Polym. Chem.* 2017, **8**, 1708-1713.

(41) N. Hazari, P. R. Melvin and M. M. Beromi, *Nat. Rev. Chem.* 2017, **1**, 0025.

(42) M. Verswyvel, C. Hoebers, J. De Winter, P. Gerbaux and G. Koeckelberghs, *J. Polym. Sci., Part A: Polym. Chem.* 2013, **51**, 5067-5074.

(43) H.-H. Zhang, Q.-S. Hu and K. Hong, *Chem. Commun.* 2015, **51**, 14869-14872.

(44) P. A. Cox, M. Reid, A. G. Leach, A. D. Campbell, E. J. King and G. C. Lloyd-Jones, *J. Am. Chem. Soc.* 2017, **139**, 13156-13165.

(45) H. L. D. Hayes, R. Wei, M. Assante, K. J. Geogheghan, N. Jin, S. Tomasi, G. Noonan, A. G. Leach and G. C. Lloyd-Jones, *J. Am. Chem. Soc.* 2021, **143**, 14814-14826.

(46) K. Kosaka, Y. Ohta and T. Yokozawa, *Macromol. Rapid Commun.* 2015, **36**, 373-377.

(47) J. A. Carrillo, M. J. Ingleson and M. L. Turner, *Macromolecules* 2015, **48**, 979-986.

(48) K.-B. Seo, I.-H. Lee, J. Lee, I. Choi and T.-L. Choi, *J. Am. Chem. Soc.* 2018, **140**, 4335-4343.

(49) H.-N. Choi, H.-S. Yang, J.-H. Chae, T.-L. Choi and I.-H. Lee, *Macromolecules* 2020, **53**, 5497-5503.

(50) J. Lee, H. Kim, H. Park, T. Kim, S.-H. Hwang, D. Seo, T. D. Chung and T.-L. Choi, *J. Am. Chem. Soc.* 2021, **143**, 11180-11190.

(51) H. Park, J. Lee, S.-H. Hwang, D. Kim, S. H. Hong and T.-L. Choi, *Macromolecules* 2022, **55**, 3476-3483.

(52) H. Kim, J. Lee, T. Kim, M. Cho and T.-L. Choi, *Angew. Chem. Int. Ed.* 2022, **61**, e202205828.

(53) B. P. Fors, D. A. Watson, M. R. Biscoe and S. L. Buchwald, *J. Am. Chem. Soc.* 2008, **130**, 13552-13554.

(54) M. Su and S. L. Buchwald, *Angew. Chem. Int. Ed.* 2012, **51**, 4710-4713.

(55) A. J. DeAngelis, P. G. Gildner, R. Chow and T. J. Colacot, *J. Org. Chem.* 2015, **80**, 6794-6813.

(56) R. P. King, S. W. Krska and S. L. Buchwald, *Org. Lett.* 2021, **23**, 7927-7932.

(57) Y. Tokita, M. Katoh, K. Kosaka, Y. Ohta and T. Yokozawa, *Polym. Chem.* 2021, **12**, 7065-7072.

(58) A. J. J. Lennox and G. C. Lloyd-Jones, *Angew. Chem. Int. Ed.* 2013, **52**, 7362-7370.

(59) C. Amatore, A. Jutand and G. Le Duc, *Chem. Eur. J.* 2011, **17**, 2492-2503.

(60) B. P. Carrow and J. F. Hartwig, *J. Am. Chem. Soc.* 2011, **133**, 2116-2119.

(61) C. F. R. A. C. Lima, A. S. M. C. Rodrigues, V. L. M. Silva, A. M. S. Silva and L. M. N. B. F. Santos, *ChemCatChem* 2014, **6**, 1291-1302.

(62) J. Jover, N. Fey, M. Purdie, G. C. Llloyd-Jones and J. N. Harvey, *J. Mol. Catal. A: Chem.* 2010, **324**, 39-47.

(63) C. P. Delaney, D. P. Marron, A. S. Shved, R. N. Zare, R. M. Waymouth and S. E. Denmark, *J. Am. Chem. Soc.* 2022, **144**, 4345-4364.

(64) J. J. Fuentes-Rivera, M. E. Zick, M. A. Düfert and P. J. Milner, *Org. Process Res. Dev.* 2019, **23**, 1631-1637.

(65) S. Ye, S. Cheng, A. A. Pollit, M. W. Forbes and D. S. Seferos, *J. Am. Chem. Soc.* 2020, **142**, 11244-11251.

(66) J. Rodriguez, H. H. Dhanjee, B. L. Pentelute and S. L. Buchwald, *J. Am. Chem. Soc.* 2022, **144**, 11706-11712.

(67) M. V. Bautista, A. J. Varni, J. Ayuso-Carrillo, C.-H. Tsai and K. J. T. Noonan, *ACS Macro Lett.* 2020, **9**, 1357-1362.

(68) S. M. Socol and J. G. Verkade, *Inorg. Chem.* 1984, **23**, 3487-3493.

(69) P. L. Arrechea and S. L. Buchwald, *J. Am. Chem. Soc.* 2016, **138**, 12486-12493.

(70) P. S. Hanley, D. Marković and J. F. Hartwig, *J. Am. Chem. Soc.* 2010, **132**, 6302-6303.

(71) P. S. Hanley and J. F. Hartwig, *J. Am. Chem. Soc.* 2011, **133**, 15661-15673.

(72) J.-N. Li, L. Liu, Y. Fu and Q.-X. Guo, *Tetrahedron* 2006, 4453-4462.

(73) M. A. Düfert, K. L. Billingsley and S. L. Buchwald, *J. Am. Chem. Soc.* 2013, **135**, 12877-12885.

(74) V. V. Grushin and H. Alper, *Organometallics* 1996, **15**, 5242-5245.

(75) E. P. Gillis and M. D. Burke, *J. Am. Chem. Soc.* 2007, **129**, 6716-6717.

(76) J. A. Gonzales, O. M. Ogba, G. F. Morehouse, N. Rosson, K. N. Houk, A. G. Leach, P. H.-Y. Cheong, M. D. Burke and G. C. Lloyd-Jones, *Nat. Chem.* 2016, **8**, 1067-1075.

(77) H. Yoshida, M. Seki, S. Kamio, H. Tanaka, Y. Izumi, J. Li, I. Osaka, M. Abe, H. Andoh, T. Yajima, T. Tani and T. Tsuchimoto, *ACS Catal.* 2020, **10**, 346-351.

(78) Y. Mutoh, Y.; K. Yamamoto and S. Saito, *ACS Catal.* 2020, **10**, 352-357.

(79) C. F. Lee, D. B. Diaz, A. Holownia, S. J. Kaldas, S. K. Liew, G. E. Garrett, T. Dudding and A. K. Yudin, *Nat. Chem.* 2018, **10**, 1062-1070.

(80) S. J. Kaldas, C.-H. Tien, G. dos Passos Gomez, S. Meyer, M. Sirvinskas, H. Foy, T. Dudding and A. K. Yudin, *Org. Lett.* 2021, **23**, 324-328.

(81) A. E. Javier, S. R. Varshney and R. D. McCullough, *Macromolecules* 2010, **43**, 3233-3237.

(82) M. A. Baker, S. F. Zahn, A. J. Varni, C.-H. Tsai and K. J. T. Noonan, *Macromolecules* 2018, **51**, 5911-5917.

(83) The polymer yields reported herein were determined after polymer precipitation, and thus could be also affected by precipitation conditions, especially with the lower molecular weight polymers (in case of incomplete precipitation, the reported yields would be lower than the actual yields obtained in polymerization reaction).

(84) S. Kobayashi, K. Fujiwara, D.-H. Jiang, T. Yamamoto, K. Tajima, Y. Yamamoto, T. Isono and T. Satoh, *Polym. Chem.* 2020, **11**, 6832-6839.

(85) Y. Yamamoto, M. Takizawa, X.-Q. Yu and N. Miyaura, *Angew. Chem. Int. Ed.* 2008, **47**, 928-931.

(86) L. P. E. Yunker, Z. Ahmadi, J. R. Logan, W. Wu, T. Li, A. Martindale, A. G. Oliver and J. S. McIndoe, *Organometallics* 2018, **37**, 4297-4308.